Microtubule-dependent intracellular trafficking promotes apical constriction during tissue invagination

Thao Phuong Le[1] and SeYeon Chung[1, *]

[1] Department of Biological Sciences, Louisiana State University, Baton Rouge, LA 70803, USA

[*]Author for correspondence: seyeonchung@lsu.edu

Abstract

The formation of an epithelial tube is a fundamental process for organogenesis. During *Drosophila* embryonic salivary gland (SG) invagination, Folded gastrulation (Fog)-dependent Rho-associated kinase (Rok) promotes contractile apical myosin formation to drive apical constriction. Microtubules (MTs) are also crucial for this process and are required for forming and maintaining apicomedial myosin. However, the underlying mechanism that coordinates actomyosin and MTs networks is still unclear. Here, we show that MT-dependent intracellular trafficking regulates apical constriction during SG invagination. Key components involved in protein trafficking, such as Rab11, Nuclear fallout (Nuf) and dynein heavy chain, are apically enriched near the SG invagination pit in a MT-dependent manner. Disruption of the MT networks or intracellular trafficking impairs apicomedial myosin formation and apical constriction. We show that MTs and dynein motors regulate Fog signaling activity. We further show that Rab11-dependent protein transport along MTs mediates clustered apical constriction during SG invagination. Key proteins that are transported include the apical determinant protein Crumbs (Crb), the key adherens junction protein E-Cadherin (E-Cad) and the scaffolding protein Bazooka/Par3. Targeted knockdown of these genes in the SG disrupts apical myosin networks and results in apical constriction defects. These results define a role of MT-dependent intracellular trafficking in regulating actomyosin networks and cell junctions, to coordinate cell behaviors during tubular organ formation.

Introduction

Formation of three-dimensional tubes by invagination of flat epithelial sheets is a fundamental process in forming organs such as the lungs and kidneys (Andrew and Ewald, 2010). To enter the third dimension, cells must change their shapes and positions relative to each other. A major cellular process during epithelial tube formation is apical constriction, a universal cell shape change that is linked to tissue bending, folding and invagination (Martin and Goldstein, 2014; Sawyer et al., 2010). During apical constriction, the apical side of an epithelial cell constricts, causing a columnar or cuboidal cell to become wedge-shaped (Martin and Goldstein, 2014; Sawyer et al., 2010). Manipulation of apical constriction in a group of cells impacts both local and global tissue shape directly, suggesting a critical role for apical constriction in forming proper tissue architecture (Chung et al., 2017; Guglielmi et al., 2015; Izquierdo et al., 2018).

Apical constriction is driven by actin filament (F-actin) networks and the molecular motor non-muscle myosin II (hereafter referred to as myosin). Over the past decade, important functions of different actomyosin structures in epithelial tissue morphogenesis have been discovered. Particularly, studies in *Drosophila* revealed a distinct population of pulsatile apical medial actomyosin (hereafter referred to as apicomedial myosin) that generates a pulling force that exerts on adherens junctions to drive apical constriction (Booth et al., 2014; Chung et al., 2017; Martin et al., 2009; Rauzi et al., 2010). In early *Drosophila* embryos, apicomedial myosin is created in response to signaling by the Folded gastrulation (Fog) ligand and its G protein-coupled receptors (GPCRs) (Kerridge et al., 2016; Manning et al., 2013), and is regulated by apical Rho-associated kinase (Rok) (Mason et al., 2013). Apical junctions and apical determinants also have an important role in the formation of functional actomyosin complexes. During *Drosophila* dorsal closure, the apical polarity regulators Par-6, aPKC and Bazooka/Par3 (Baz/Par3) (altogether known as the Par complex) regulate pulsed actomyosin contractions in amnioserosa cells (David et al., 2010). In the *Drosophila* embryonic trachea, the apical protein Crumbs (Crb) is required for proper organization of the actomyosin complex (Letizia et al., 2011).

72 Emerging evidence suggests that microtubules (MTs) play a critical role in tissue
73 invagination (Booth et al., 2014; Ko et al., 2019). MTs serve as tracks in intracellular
74 transport, raising the possibility that MTs regulate apical constriction through the endo-
75 and exocytosis of membrane receptors and adhesion molecules (Khanal et al., 2016; Le
76 Droguen et al., 2015). Several lines of evidence suggest the importance of the endocytic
77 pathway, including the molecular motor dynamin and the vesicle trafficking Rab proteins,
78 in apical constriction in both in vitro and in vivo systems. During *Xenopus* gastrulation,
79 disrupting endocytosis with dominant-negative dynamin or Rab5 perturbs apical
80 constriction and invagination of cell sheets (Lee and Harland, 2010). During *Drosophila*
81 gastrulation, the apical surface of cells is reshaped via Rab35 and RabGEF Sbf, which
82 direct the plasma membrane to Rab11-positive recycling endosomes through a dynamic
83 interaction with Rab5 endosomes to reshape actomyosin networks (Miao et al., 2019).
84 Moreover, in the developing neural tube in *Xenopus*, asymmetric enrichment of Rab11 at
85 the medial apical junctions is critical for apical constriction, suggesting that membrane
86 trafficking has a key role in apical constriction (Ossipova et al., 2014). However, exactly
87 how membrane trafficking, MTs, and actomyosin networks are linked remains to be
88 discovered.

89 To determine how these three cellular attributes contribute to tissue invagination, we use
90 the *Drosophila* embryonic salivary gland (SG) as a model. We and others showed that
91 apical constriction is regulated in a highly coordinated and spatiotemporally controlled
92 manner during epithelial tube formation (Booth et al., 2014; Chung et al., 2017; Myat and
93 Andrew, 2000; Sanchez-Corrales et al., 2018). The *Drosophila* embryo forms two SG
94 tubes via invagination of two epithelial placodes on the ventral surface (Chung et al.,
95 2014). Before invagination, a small group of cells in the dorsal/posterior region of each
96 SG placode begin to constrict. As those cells internalize to form the invagination pit, more
97 cells anterior to the pit undergo clustered apical constriction in a Fog signaling-dependent
98 manner (Chung et al., 2017) (Fig. 1A). In the absence of *fog*, SG cells fail to accumulate
99 Rok and myosin in the apicomedial region of the cells. MTs aid in the formation and
100 maintenance of the apicomedial myosin network during SG invagination (Booth et al.,
101 2014). The MT cytoskeleton near the invagination pit forms a network of longitudinal MT
102 bundles, with the minus ends of MTs facing the apical domain of the cells and interacting

with the apicomedial myosin (Booth et al., 2014). Disruption of MTs causes loss of apicomedial myosin and disrupted apical constriction during SG invagination (Booth et al., 2014). However, it is still unknown how intracellular trafficking affects these two processes.

In this study, we demonstrate that key proteins involved in intracellular trafficking - including Rab11, its binding partner Nuclear fallout (Nuf), and dynein heavy chain - are enriched in the apical domain of SG cells during invagination. Moreover, this accumulation is MT-dependent. Our data suggest that apical transport of several proteins, including the apical determinant protein Crb, the key adherens junction protein E-Cadherin (E-Cad), and the scaffolding protein Baz/Par3, is compromised when the MT networks are disrupted. We further show that disruption of MTs or reducing dynein heavy chain leads to a decrease of Rok and myosin in the apical domain and causes uncoordinated apical constriction in the SG. Altogether, our work mechanistically links MT-dependent intracellular trafficking to the regulation of actomyosin networks during tubular organ formation.

Results

Intracellular trafficking components are apically enriched near the invagination pit

To test a role for the intracellular trafficking machinery in spatially biased signaling activation and protein accumulation during SG invagination, we analyzed the subcellular localization of proteins that are involved in vesicle trafficking in the SG. Several endosome markers were tested, including Rab5 (an early endosome marker) (Gorvel et al., 1991), Rab7 (a late endosome marker) (Meresse et al., 1995; Wichmann et al., 1992), Rab11 (a recycling endosome marker) (Ullrich et al., 1996), Nuclear fallout (Nuf, a putative binding partner for Rab11) (Riggs et al., 2003), and Sec15 (an exocyst complex component and effector for Rab11) (Langevin et al., 2005; Zhang et al., 2004). We observed enrichment of Rab11, Nuf, and Sec15 at and near the SG invagination pit, suggesting active trafficking activities in the region where cells are apically constricting (Figs. 1C-D', G-H';

131 Figs. S1A-C). Compared to a more uniform distribution of Rab11 and Nuf in the entire
132 apical domain, Sec15 signals appeared to be enriched at adherens junctions (Fig. S1B).
133 Using labeling with E-Cad, an adherens junction marker, and CrebA, a SG nuclear
134 marker, we segmented apical cell outlines (Figs. 1B,B'). Intensity mean of Rab11 or Nuf
135 in the apical domain of each cell showed a negative correlation with the apical area of
136 cells in the entire SG (Fig. 1E), further supporting the conclusion that increased trafficking
137 and apical constriction are closely linked.

138 Rab5, an early endosome marker, was also upregulated near the invagination pit,
139 suggesting active endocytosis in this region (Figs. S1B,B'). Dynein heavy chain, a subunit
140 of the dynein motor complex that transports cargos along MTs toward their minus ends,
141 also showed upregulation near the invagination pit (Figs. 1J,J'). Rab7, a late endosome
142 marker, however, did not show any enrichment but localized as large punctate structures
143 in the cytoplasm of the entire SG placode (Figs. 1L,L'), suggesting that trafficking from
144 early to late endosomes or between late endosomes to lysosomes is not upregulated
145 near the pit during SG invagination. Overall, our results suggest active intracellular
146 trafficking, possibly both endo- and exocytosis, near the invagination pit during SG
147 invagination.

148

149 **MT-dependent vesicular transport is required for apical constriction in the SG**

150 Strong apical enrichment of Rab11 and Nuf in the SG cells near the invagination pit led
151 us to test whether these vesicle markers are associated with vertically aligned MTs that
152 could facilitate their polarized distribution. As in many epithelial cells, MT minus- and plus-
153 ends face the apical and the basal domain of the SG cells, respectively (Booth et al.,
154 2014; Myat and Andrew, 2002). Indeed, co-immunostaining of tyrosinated α-tubulin, a
155 marker of dynamic or newly polymerized MTs, and Rab11 showed a partial overlap of the
156 two proteins at the apical region of the SG cells (Figs. 2A'-B''). Mander's overlap
157 coefficients of Rab11 and tyrosinated α-tubulin revealed that 59% of Rab11 signals
158 overlapped with tyrosinated α-tubulin labeling and 34% of tyrosinated α-tubulin signals
159 co-localized with Rab11 signals (Fig. 2C).

160 To test whether Rab11 apical enrichment in SG cells is dependent on MT networks, we
161 disrupted MTs in the SG by overexpressing spastin, a MT-severing protein (Sherwood et
162 al., 2004), using the SG-specific *fkh-Gal4* driver. In control SGs, tyrosinated α-tubulin and
163 acetylated α-tubulin, a marker of stable and longer-lived MTs (Westermann and Weber,
164 2003), were observed abundantly in the apical domain of cells in the whole placode (Figs.
165 2D'',D'''; Fig. S2). In spastin-overexpressing SGs, both tyrosinated and acetylated α-
166 tubulin signals were strongly reduced, revealing loss of MT filaments (Booth et al., 2014)
167 (Figs. 2E'',E''',S2B''); the upregulation of Rab11 near the invagination pit (Fig. 2D') was
168 also abolished and Rab11 was mislocalized basolaterally (Figs. 2E',F'). Quantification of
169 Rab11 localization showed that SGs with disrupted MTs showed much lower intensity in
170 the apical domain near the invagination pit compared to control SGs (Fig. 1C' versus Fig.
171 2G'). Similar patterns were observed for Nuf (Figs. 2F-H). These data suggest that MT
172 networks are required for apical enrichment of Rab11 and Nuf during SG invagination.

173 We next asked if specific modulation of Rab11 levels could compromise apical
174 constriction. To test this possibility, we disrupted the function of Rab11 by overexpressing
175 a dominant-negative form of Rab11 (Rab11S25N-YFP; hereafter referred to as Rab11-
176 DN) in the SG. Compared to controls (Fig. 3A), SGs overexpressing Rab11-DN showed
177 more cells with larger apical area (Fig. 3B,F), suggesting a role for Rab11 in apical
178 constriction during SG invagination.

179 As dynein heavy chain was also enriched near the invagination pit (Figs. 1J,J''), we
180 hypothesized that dynein motors may traffic key proteins along MTs to control apical
181 constriction during SG invagination. Indeed, zygotic knockdown of *Dynein heavy chain*
182 *64C* (*Dhc64C*) in the SG resulted in more cells with larger apical areas during
183 invagination, suggesting defective apical constriction (Figs. 3C,C',F). Since *Dhc64C* has
184 strong maternal expression and is essential for oogenesis and early embryo development
185 (Li et al., 1994), we tried to reduce Dhc64C levels still further by knocking down *Dhc64C*
186 both maternally and zygotically, using a maternal driver *matα-Gal4* along with the SG-
187 specific *fkh-Gal4*. Embryos with reduced maternal and zygotic pools of Dhc64C showed
188 a range of morphological defects in the entire embryo, some of which were severely
189 distorted (data not shown). In embryos with more subtle morphological defects, SG cells

still invaginated and formed a tube. However, SGs showed a range of phenotypes, from relatively normal but with slightly larger apical areas in individual cells (Fig. 3G; mild), to an enlarged invagination pit (Fig. 3G; intermediate), to quite distorted (Fig. 3G; severe).

Klarsicht (Klar), the *Drosophila* Klarsicht-Anc-Syne Homology (KASH) domain protein, mediates apical transport in the SG (Myat and Andrew, 2002) via the MT motor cytoplasmic dynein (Gross et al., 2000). We therefore predicted that *klar* would also influence apical constriction during SG invagination. Indeed, *klar* mutant embryos showed SGs with mild apical constriction defects compared to wild type controls (Figs. 3D-E',F). Overall, our data suggest essential roles of Rab11 trafficking and MT- and dynein-dependent transport in regulating apical constriction during SG invagination.

Compromised intracellular trafficking leads to failure in accumulation of apicomedial Rok and reduction of apicomedial myosin formation in SG cells

The apicomedial myosin structure generates the pulling force to drive apical constriction in SG cells (Booth et al., 2014; Chung et al., 2017), and spastin overexpression inhibits formation of apicomedial myosin during SG invagination (Booth et al., 2014). We therefore tested whether apicomedial myosin formation is affected in SG cells when dynein-dependent transport is compromised. In control SGs, sqh-GFP (a functional GFP-tagged version of the myosin regulatory light chain) (Royou et al., 2004) showed a strong apicomedial myosin web in constricting cells near the invagination pit (Figs. 4A-A''''). Knockdown of *Dhc64C* caused a significant reduction of apicomedial myosin (Figs. 4B-B'''' and C), suggesting its role in forming and/or maintaining apicomedial myosin.

Consistent with previous studies (Chung et al., 2017; Roper, 2012), a myosin pool that is closely associated with adherens junctions, junctional myosin, also showed strong signals in wild type SG cells, often with stronger signals at vertices (Fig. 4A-A'''). Intriguingly, the intensity of junctional myosin was also reduced upon *Dhc64C* knockdown (Fig. 4B-B''' and C). The ratio of apicomedial to junctional myosin was significantly reduced in *Dhc64C* RNAi SGs (Fig. 4C), suggesting a more significant effect on apicomedial than on

218 junctional myosin upon *Dhc64C* knockdown. Similar to *Dhc64C* knockdown, reduction of
219 apicomedial and junctional myosin was observed in *klar* mutant SGs (Figs. 4D-F). Our
220 data suggests that defective apical constriction in *Dhc64C* RNAi and *klar* mutant SGs
221 could be due to failure in proper organization of myosin structures, primarily in the
222 apicomedial region of SG cells.

223 We previously showed that Fog signaling-dependent accumulation of apical medial Rok
224 is required for apicomedial myosin formation for coordinated apical constriction in SG
225 cells (Chung et al., 2017). To test whether Rok accumulation is dependent on MTs, we
226 quantitatively analyzed Rok distribution using a ubiquitously expressed GFP-tagged Rok
227 transgene (Rok-GFP) (Abreu-Blanco et al., 2014) in wild type and MT-disrupted SGs.
228 Disruption of MTs by overexpression of spastin abolished the apicomedial accumulation
229 of Rok in cells near the invagination pit, found in control SGs (Figs. 5A-B'' and G).

230 We also tested for accumulation of apicomedial Rok-GFP signals in *Dhc64C* RNAi and
231 *klar* mutant SGs. Similar to spastin overexpression, reduction of *Dhc64C* levels led to
232 more dispersed Rok signals along the apical domain of SG cells near the pit (Fig. 5C-C''
233 and G). In *klar* mutants, Rok-GFP tended to accumulate less profoundly and less
234 uniformly in the apicomedial region of SG cells (Figs. 5E-E'') although not statistically
235 significant compared to control (Fig. 5H). Overall, our data suggest that dynein-dependent
236 intracellular trafficking along MTs regulates apical accumulation of Rok and apicomedial
237 myosin formation during SG invagination.

238

239 **Fog signaling activity is reduced when MTs are disrupted**

240 Since Rok accumulation, apicomedial myosin formation, and subsequent coordinated
241 apical constriction in the SG are Fog-dependent (Chung et al., 2017), we tested whether
242 the roles of Fog signaling and MT trafficking in apical constriction were dependent on
243 each other. Although the existing Fog antibody (Fuse et al., 2013) detected the
244 endogenous Fog protein in the SG lumen at later stages, the signals at stage 11 were not
245 strong enough to show precise subcellular localization of Fog in the SG. We therefore

246 overexpressed Fog in the SG to saturate the transport system and test a role of MTs in
247 transporting Fog in this sensitized background. Consistent with our previous data that Fog
248 signal mediates apicomedial Rok accumulation and apicomedial myosin formation
249 (Chung et al., 2017), Fog-overexpressing SG cells over-accumulated Rok in the
250 apicomedial region and dramatically increased apicomedial myosin (Figs. 6B,B'). This
251 Fog gain-of-function effect on over-accumulation of Rok and increased apicomedial
252 myosin was suppressed by spastin overexpression or *Dhc64C* knockdown (Figs. 6C-D',
253 G-H',J,L). Interestingly, we also observed highly ruffled SG cell junctional morphology in
254 almost all SG cells when Fog was overexpressed (Figs. 6I,I'). Similar cell distortions,
255 albeit in a moderate level, have been observed during apical constriction in mesodermal
256 cells (Martin et al., 2009) and in SG cells (Chung et al., 2017) when apicomedial myosin
257 exerts the pulling force on adherens junctions. Indeed, increased apicomedial myosin
258 was connected with E-Cad signals at distorted cell junctions (Figs. 6I,I'), suggesting that
259 this ruffled junctional phenotype is due to increased pulling forces generated by high
260 levels of apicomedial myosin upon increased Fog signaling activity. This convoluted
261 junctional phenotype was suppressed by spastin overexpression or *Dhc64C* knockdown
262 (Figs. 6G-H',K). Taken together, our data suggest that MTs and intracellular trafficking is
263 necessary for Fog signaling activity and its downstream targets Rok and myosin, possibly
264 by regulating transport of a key Fog signaling component(s) during SG invagination.

265

266 **Enrichment of key apical and junctional proteins is MT-dependent and is required**
267 **for apical constriction during SG invagination**

268 Transport of several key apical and junctional proteins is dependent on MTs and Rab11
269 (Jouette et al., 2019; Khanal et al., 2016; Le Droguen et al., 2015). One such protein is
270 an apical transmembrane protein Crb, and Rab11 helps maintain apical Crb in the
271 *Drosophila* ectoderm (Roeth et al., 2009). In the *Drosophila* SG and follicle cells, Crb is
272 apically transported along MTs by the dynein motor (Myat and Andrew, 2002) (Aguilar-
273 Aragon et al., 2019). Importantly, in *Drosophila* tracheae, loss of *crb* impairs apical
274 constriction during the internalization process (Letizia et al., 2011). Two key junctional

275 proteins, E-Cad and Baz/Par3, are also trafficked by MTs in *Drosophila* embryonic
276 trachea (Le Droguen et al., 2015). During apical constriction, contractile forces generated
277 by the actomyosin complex are exerted on adherens junctions, with E-Cad being a core
278 component that integrates contractile forces to generate tension (Martin et al., 2009).
279 During amnioserosa apical constriction at *Drosophila* dorsal closure, Baz/Par3 in the Par
280 complex regulates pulsed actomyosin contractions (David et al., 2010).

281 We therefore asked if MTs have a role in trafficking Crb, E-Cad and Baz apically in the
282 SG during invagination. Consistent with previous studies (Myat and Andrew, 2002; Roper,
283 2012), Crb was upregulated near the invagination pit during SG invagination (Fig. 7A). E-
284 Cad and Baz were also upregulated near the invagination pit (Figs. 7A',E). Disruption of
285 MTs resulted in reduction of Crb, E-Cad and Baz signals compared to control (Fig. 7A-
286 B'',E-I). Moreover, spastin overexpression caused discontinuous Crb signals along the
287 junctions (Fig. 7D). Whereas the number of gaps was not significantly different between
288 control and spastin-overexpressing SGs (Fig. 7K), quantification of the ratio of length of
289 gaps to junctional length revealed increased gap length in spastin-overexpressing SGs
290 (Fig. 7J). These data suggest that apical transport of Crb, E-Cad and Baz in the SG is
291 dependent on MTs.

292 We further tested MT-dependent apical transport of Crb in the SG using the same genetic
293 suppression strategy as we used for testing a role of MTs in Fog trafficking (Figs. 6C-C').
294 We co-overexpressed Crb and spastin in the SG to test whether disruption of MTs affects
295 apical transport of Crb. A similar approach was taken in a recent study, where
296 overexpression of Crb provided a highly sensitive genetic background for identifying
297 components involved in Crb trafficking (Aguilar-Aragon et al., 2019). Consistent with
298 previous findings that Crb expression expands apical membranes in epithelial cells
299 (Chung and Andrew, 2014; Chung et al., 2017; Myat and Andrew, 2002; Wodarz et al.,
300 1993), overexpression of Crb resulted in enlarged apical areas of SG cells during
301 invagination (Figs. S4B-B'). Unlike control SG cells, Crb-overexpressing SG cells also
302 showed over-accumulation of Crb on the apical surface (Figs. S4A-B'). Co-
303 overexpression of spastin and Crb suppressed this accumulation of Crb (Figs. S4C,C'),
304 further supporting the idea that apical transport of Crb in the SG is dependent on MTs.

305 To test for a role of Crb, E-Cad and Baz in regulating apical constriction during SG
306 invagination, we knocked down each gene in the SG using RNAi. Knockdown of *crb, E-*
307 *Cad* or *baz* resulted in reduction of junctional Crb, E-Cad or Baz levels, respectively,
308 compared to control (Figs. S3A-C''). Reduction of *crb*, *E-Cad* or baz increased the number
309 of cells that have larger apical areas compared to control (Figs. 7L-N'). Quantification of
310 the percentage of cells and cumulative percentage of cells of different apical areas
311 showed a significant decrease in the number of constricting cells in *crb* and *baz*
312 knockdown SGs (Fig. 7O). *E-Cad* knockdown SGs also displayed a similar trend although
313 with less statistical significance (Fig. 7O). Overall, our data suggest a role of Crb, E-Cad
314 and Baz in regulating apical constriction during SG invagination.

315

316 **Apical trafficking of Crb, E-Cad and Baz is MT- and Rab11-dependent in the SG**
317 **throughout development**

318 To further investigate the role of MTs in apical trafficking of Crb, E-Cad and Baz in the
319 SG, we overexpressed spastin throughout development and analyzed late stage SGs,
320 where apical trafficking is more easily detected in elongated SG cells. Analysis of spastin-
321 overexpressing SGs at stage 16 revealed that disruption of MTs resulted in short SG
322 tubes with a thin lumen compared to control SGs of the same stage (Figs. S5A,B).
323 Strikingly, whereas the majority of Rab11- and Nuf-positive vesicles localized in the apical
324 region of control SG cells (Figs. S5A-A'''), Rab11 and Nuf were observed as large
325 aggregates in the cytoplasm in spastin-overexpressing cells, overlapping with each other
326 (Figs. S5B-B'''). Our data suggest that MTs are required for apical enrichment of
327 Rab11/Nuf vesicles throughout SG tube formation.

328 Using the same co-overexpression strategy that we used for stage 11 (Figs. S4B-C'), we
329 tested whether MTs and Rab11 are required for apical trafficking of Crb, E-Cad and Baz
330 also at stage 16. Consistent with previous studies (Chung and Andrew, 2014; Wodarz et
331 al., 1993), Crb overexpression in the SG caused a dramatic increase of the apical
332 membrane as well as mislocalization of Crb basolaterally along the entire membrane
333 (Figs. S5C-C'''). Overexpression of E-Cad alone using UAS-Shotgun-GFP (Shg,

334 *Drosophila* E-Cad; Rorth, 2014) did not result in overt morphological defects in the SG,
335 and punctate E-Cad signals mostly overlapped with Nuf signals at and near adherens
336 junctions (Figs. S5E-E'''). Overexpression of Baz using UAS-Baz-GFP (Benton and St
337 Johnston, 2003) in the SG caused a slightly enlarged lumen (Fig. S5G-G'''). Baz-GFP
338 signals were detected mostly at adherens junctions, but small punctate structures were
339 also detected in the cytoplasm (Fig. S5G').

340 Co-overexpression of spastin along with Crb or Baz suppressed the overexpression
341 phenotypes for Crb or Baz (Figs. S5D-D''',H-H''). Importantly, in SGs that co-
342 overexpressed spastin along with any of these three apical/junctional proteins, each
343 protein mislocalized as cytoplasmic aggregates near the basolateral domain, which were
344 largely overlapping with mislocalized Rab11/Nuf (Figs. S5D-D''',F-F''',H-H'''). Overall, our
345 data suggest that several key proteins, including Crb, E-Cad and Baz, are trafficked
346 apically in a MT- and Rab11-dependent manner in the SG throughout tube formation.

347

348 **Reducing apical and junctional proteins affects Rok accumulation and apicomedial**
349 **myosin formation**

350 To test whether apical constriction defects observed in *crb*, *E-Cad* and *baz* knockdown
351 SGs (Figs. 7L-O) are linked to apicomedial myosin formation, we analyzed myosin levels
352 in SGs with these knockdowns. Overall myosin levels were reduced in *crb* or *baz*
353 knockdown SGs, both in the apicomedial region and at adherens junctions (Figs. 8A-
354 A'',B-B'',D-D'',E). The ratio of apicomedial to junctional myosin was also reduced (Fig.
355 8E), suggesting that apical constriction defects in SGs depleted of *crb* or *baz* are, at least
356 in part, due to failure of apicomedial myosin formation. In SGs depleted of *E-Cad*, myosin
357 levels at each domain did not change significantly, but the ratio of apicomedial myosin to
358 junctional myosin was significantly reduced compared to control (Fig. 8C-C'',E).
359 Therefore, the apical constriction defects caused by *E-Cad* knockdown might be due to
360 an imbalance of contractile forces.

361 Knockdown of *crb* or *baz* also resulted in Rok-GFP signals less accumulating in the apical
362 region of cells near the invagination pit (Figs. 8G-I''). Quantification of the areas occupied
363 by Rok-GFP puncta showed significant reduction in accumulation of apicomedial Rok
364 when *crb* or *baz* was knocked down (Fig. 8J). Consistent with the relatively mild effect of
365 *E-Cad* knockdown on apicomedial myosin (Figs. 8C-C'',E), Rok accumulation was not
366 significantly affected by *E-Cad* knockdown. Several SG cells, however, showed dispersed
367 Rok-GFP signals in cells near the invagination pit, which was not observed in control cells
368 (Figs. 8 H-H'',J), suggesting some defects in Rok accumulation. Taken together, our
369 results suggest a role for Crb and Baz in regulating apical constriction by mediating Rok
370 accumulation and myosin activation during SG invagination.

371

372 **Discussion**

373 **MT-dependent intracellular trafficking during apical constriction**

374 Using the *Drosophila* SG, we demonstrate that MT-dependent intracellular trafficking is
375 critical for apical constriction during tissue invagination. MTs have been shown to have a
376 crucial role in stabilizing apical myosin during epithelial morphogenesis both in early
377 *Drosophila* embryos and in the *Drosophila* SG (Booth et al., 2014; Ko et al., 2019).
378 Particularly in the SG, MTs interact with apicomedial myosin via Short stop, the
379 *Drosophila* spectraplakin, emphasizing a direct interplay between the MT and the apical
380 myosin networks (Booth et al., 2014). Our data reveals another role of MTs in regulating
381 protein trafficking to control the apical myosin networks during tissue invagination. During
382 SG invagination, a network of longitudinal MT bundles is observed near the invagination
383 pit (Booth et al., 2014). Our data shows apical enrichment of key endocytic markers in the
384 same area and that this enrichment is important for forming the apicomedial myosin
385 networks (Figs. 1-4), suggesting a link between localized protein trafficking along MTs to
386 apical myosin regulation. Our data support a model that dynein- and Rab11-dependent
387 intracellular trafficking is crucial for organizing apical myosin networks during apical
388 constriction in the SG.

389 Interestingly, cytoplasmic dynein is associated with cellular structures and exerts tension
390 on MTs. For example, dynein tethered at the cell cortex can apply a pulling force on the
391 MT network by walking towards the minus end of a MT (Laan et al., 2012). In interphase
392 cells, force generated by dynein also regulates MT turnover and organization (Yvon et
393 al., 2001). Therefore, we do not rule out the possibility that reduced dynein functions could
394 affect MT organization and/or a pulling force on the MT networks regardless of its role in
395 intracellular trafficking, which will subsequently affect apical myosin structures during SG
396 invagination. However, we favor the apical trafficking model as we did not observe overt
397 changes in the MT networks in *Dhc64C* RNAi SGs (data not shown).

398

399 **Integrating apical and junctional proteins with actomyosin networks during SG**
400 **invagination**

401 During branching morphogenesis in *Drosophila* trachea, MTs and dynein motors have a
402 critical role in proper localization of junctional proteins such as E-Cad and Baz (Le
403 Droguen et al., 2015). This is consistent with our observations with MT-dependent
404 trafficking of Crb, E-Cad and Baz in both early (Fig. 7) and late stage SG (Fig. S5),
405 suggesting a conserved role of MT-dependent intracellular trafficking in junctional
406 remodeling and stabilization during epithelial tube formation. Our data suggests that
407 proper levels of apical and junctional proteins are also important for tissue invagination at
408 the beginning of epithelial tube formation. Dispersed Rok and less prominent apicomedial
409 myosin are observed in invaginating SGs upon knockdown of *crb*, *E-Cad* and *baz* (Fig.
410 8), suggest a requirement of apical and junctional proteins in proper organization of apical
411 actomyosin networks during epithelial tube formation. We propose that MTs and Rab11
412 play a role in apical trafficking of these proteins during SG invagination and throughout
413 SG tube formation. Alternatively, MTs have a role in assembling/anchoring these apical
414 components, through regulation of unidentified molecules. Recent studies in *Drosophila*
415 mesoderm invagination showed that MTs help to establish actomyosin network linked to
416 cell junction to facilitate efficient force transmission to promote apical constriction (Ko et
417 al., 2019). In Ko et al., (2019), however, MT-interfering drugs and RNAi of CAMSAP end-

binding protein were used to prevent MT functions and the effect cannot be directly compared to our data where spastin was used to sever existing MTs. Further work will be needed to directly monitor MT-dependent transport of Crb, E-Cad and Baz during SG invagination and clarify the mechanism.

When *crb* is knocked down using RNAi in the SG, overall intensity of myosin is decreased near the invagination pit, for both apicomedial and junctional pools (Fig. 8). It is possible that proper Crb levels are required for modulating myosin activity both in the apical domain and at junctions, which contribute to apical constriction and cell rearrangement during SG invagination. Anisotropic localization of Crb and myosin was observed at the boundary of the SG placode, where myosin accumulates at edges where Crb is lowest (Roper, 2012). Planar polarization of Rok at this boundary is modulated through phosphorylation by Pak1 downstream of Crb (Sidor et al., 2020). It will be interesting to further test how Crb might affect junctional myosin dynamics and SG invagination.

As contractile actomyosin structures exert forces on adherens junction to drive apical constriction, we speculate that slight reduction of apicomedial myosin upon *E-Cad* RNAi might be due to reduction of cell adhesion. Also, decrease of apicomedial and junctional myosin caused by *baz* knockdown is consistent with the role of the Par complex in regulating pulsed actomyosin contraction during *Drosophila* dorsal closure (David et al., 2010). It will be interesting to determine if coordination of apical and junctional proteins and apical cytoskeletal networks through intracellular trafficking is conserved during tubular organ formation in general.

Regulation of Fog signaling activity

The Fog pathway represents one of the best-understood signaling cascades controlling epithelial morphogenesis (Manning and Rogers, 2014). Although best studied in *Drosophila*, the pathway components have been also identified in other insects, suggesting a more widely conserved role of Fog signaling in development (Benton et al., 2019; Urbansky et al., 2016). The dorsal/posterior region of the SG where Dhc64C is

446 apically enriched (Fig. 1) correlates with localized Fog signaling activity that promotes
447 clustered apical constriction (Chung et al., 2017). Disruption of MTs or *Dhc64C*
448 knockdown not only causes dispersed Rok and defective apicomedial myosin (Fig. 5),
449 which is reminiscent of *fog* mutant phenotypes, but also suppresses the Fog gain-of-
450 function effect on Rok and myosin (Fig. 6). We propose that dynein-dependent apical
451 trafficking is important for regulating Fog signaling activity to control apical constriction
452 during epithelial tube formation, with the Fog ligand and/or the as yet unidentified SG
453 receptor(s) of Fog being possible cargos of dynein.

454 Apical enrichment of Rab11/Nuf is also MT-dependent during SG invagination and
455 disruption of the Rab11 function inhibits apical constriction in SGs (Fig. 3). Unlike other
456 apical or junctional proteins that we have tested (Crb, E-Cad and Baz) that colocalize with
457 Rab11/Nuf when mislocalized, mislocalized Fog did not co-localize with Rab11 or Nuf
458 (Fig. S6). It could be explained by the fact that Rab11 is primarily associated with recycling
459 endosomes; when Fog is not used, it is most likely degraded rather than recycled. As
460 recycling of membrane receptors to the cell surface plays an important role in the
461 regulation of overall signaling activity, it is possible that Rab11 is also involved in recycling
462 of the Fog receptor(s) to regulate Fog activity in the SG. Indeed, several GPCRs are
463 recycled via Rab11 (Anborgh et al., 2000; Cerniello et al., 2017; Dale et al., 2004; Fan et
464 al., 2003; Hamelin et al., 2005; Hunyady et al., 2002; Innamorati et al., 2001; Volpicelli et
465 al., 2002). Further work needs to be done to fully understand the mechanisms underlying
466 trafficking of Fog and its receptor(s) and how the signaling pathway is able to generate
467 cellular forces to drive cell shape changes during epithelial morphogenesis.

468

469 **Materials and Methods**

470 **Fly stocks and husbandry**

471 Fly lines used in our experiments were listed in a separate table. All crosses were
472 performed at 25°C, unless stated otherwise.

473

474 **Antibody staining and confocal microscopy**

475 Antibodies used in our experiments were listed in a separate table. Embryos were
476 collected on grape juice-agar plates and processed for immunofluorescence using
477 standard procedures. Briefly, embryos were dechorionated in 50% bleach, fixed in 1:1
478 heptane:formaldehyde for 40 min and devitellinized with 80% EtOH, then stained with
479 primary and secondary antibodies in PBSTB (1X PBS, 0.1% Triton X-100, 0.2% BSA).
480 For acetylated α-tubulin, tyrosinated α-tubulin staining, embryos were hand-devitellinized.
481 All images were taken with a Leica SP8 confocal microscope.

482

483 **Cell segmentation and apical area quantification**

484 Embryos immunostained with E-Cad and CrebA were imaged using a Leica SP8 confocal
485 microscope. Since Rok accumulation, apicomedial myosin and apical constriction depend
486 on the depth of invagination in the SG, SGs that were invaginated within the range of 5.1-
487 9.9 μm depth were used for quantification for proper comparison between different
488 genotypes. Maximum intensity projection was generated from three apical focal planes
489 with highest E-Cad signals for all genotypes, except for maternal/zygotic knockdown of
490 *Dhc64C*, where 10 to 30 focal planes were used due to wavy epithelial morphology (0.3
491 μm apart for each focal plane). Cells were segmented along the E-Cad signals and cell
492 areas were calculated using the Imaris Program (Bitplane). Since the Imaris Program
493 calculated the areas of both the front and the back of the projected cell layer, we divided
494 the measured areas by two to get the true values of apical areas of SG cells.

495

496 **Negative correlation between apical area and Rab11/Nuf intensity**

497 Cell segmentation for five WT SGs within the range of 5.1- 9.9 μm invagination was
498 performed as described above. All experiments were carried out in the same condition
499 and the same setting for confocal imaging was used. Intensity mean was measured for
500 the entire Rab11/Nuf signals for each segmented cell using the Imaris Program (Bitplane)

501 and plotted. Correlation (Pearson) and P values were calculated using the GraphPad
502 Prism software.

503 To compare the enrichment of Rab11/Nuf near the invagination pit of the WT SG to the
504 spastin overexpressed SG, the ratio of deviation of Rab11/Nuf intensity to median
505 Rab11/Nuf intensity was used. Median value of Rab11/Nuf intensity is the average of
506 Rab11/Nuf mean intensities in all SG cells. Deviation of Rab11/Nuf intensity is the
507 difference between the mean intensity of each cell and the median value. Five WT SGs
508 (690 cells) and four spastin-overexpressed SGs (396 cells) were analyzed and plotted. P
509 values were calculated using the Mann-Whitney U test in the GraphPad Prism software.

510

511 **Colocalization analysis**

512 Colocalization analyses were performed with the JACOP plugin in Fiji software.
513 Thresholded Manders' overlap coefficients were used to show the extent to which two
514 proteins colocalize. Manders' coefficients, vary from 0 to 1, are indicators of overlap
515 between two proteins and are independent of signal proportionality. The Manders' overlap
516 coefficient for Rab11 is the proportional Rab11 that is colocalized with tyrosinated α-
517 tubulin. The Manders' overlap coefficient for tyrosinated α-tubulin is the proportional
518 tyrosinated α-tubulin that is colocalized with Rab11. For each SG, the dorsal/posterior
519 region of 100 μm^2 where Rab11 is upregulated was tested. Six WT embryos were used
520 for quantification.

521

522 **Quantification of the intensity of myosin, Crb, E-Cad and Baz**

523 A group of 30 (for control and spastin-overexpressing SGs in Fig. 7) or 10 (for all other
524 genotypes) cells in the dorsal/posterior region of SG placode near the invagination pit
525 were selected for quantification. For myosin quantification, maximum intensity projections
526 that span the apical and the junctional region of SG cells were used (Leica LasX) and
527 measurements were performed using the Fiji software. Regions were drawn manually

528 along the inner or outer boundary of E-Cad signals of each cell to calculate the mean
529 intensity of apicomedial and junctional myosin. For background correction, mean intensity
530 of apicomedial myosin in ten cells outside of the SG placode was measured. The average
531 value of mean intensities of apicomedial myosin in these ten cells was used to subtract
532 the background of the cells inside the placode from the same embryo. For each genotype,
533 five SGs were used for quantification. P values were calculated using the Mann-Whitney
534 U test in the GraphPad Prism software. Mean intensities of Crb, E-Cad and Baz were
535 measured with the same method used for quantifying the mean intensity of junctional
536 myosin.

537

538 **Quantification of area of Rok puncta**

539 A single confocal section that had the strongest medial Rok signals was selected. Cell
540 boundaries were labeled by immunostaining with the antibody against E-Cad. To analyze
541 Rok distribution, we performed particles analysis using the Fiji software. 15 cells in the
542 dorsal/posterior region near the invagination pit were selected for quantification. Rok-GFP
543 signals were converted into black-and-white using the *Threshold* tool in Photoshop before
544 analysis. Using the *Analyze particles* tool in Fiji, Rok-GFP puncta with areas equal or
545 larger than 0.02 μm^2 were measured. Five SGs were used for quantification. P values
546 were calculated using the Mann-Whitney U test in the GraphPad Prism software.

547

548 **Quantification of tortuosity**

549 10 cells in the dorsal/posterior region near the invagination pit of the SG placode were
550 selected for quantification. Using the Fiji software, the actual length of a given adherens
551 junction (L) was calculated using the E-Cad signals. The tortuosity was calculated as the
552 ratio of the junctional length (L) and the shortest distance (L_o) between the two vertices
553 (tortuosity= L/L_o). Five SGs were used for quantification for each genotype. P values were
554 calculated using the Mann-Whitney U test in the GraphPad Prism software.

555

556 **Quantification of length and number of gaps of junctional Crb**

557 Length of gaps and junctional length were measured using the Fiji software. Gaps that
558 have the length equal or more than 0.2 μm were quantified. If there were more than one
559 gap per junction, the length of gaps was calculated as a sum of all gaps in a given junction.
560 For each SG, 10 cells in the dorsal/posterior region were used for quantification. For the
561 number of gaps, the total number of gaps in those 10 cells were counted. Four SGs (~90
562 junctions) were used for quantification.

563

Fly strains	**Source**	**RRID**	**References**
Rab11-EYFP	Bloomington Stock Center	62549	(Dunst et al., 2015)
Rab5-EYFP	Bloomington Stock Center	62543	Dunst et al., 2015
Rab7-EYFP	Bloomington Stock Center	62545	Dunst et al., 2015
UAS-Spastin (on II)	N. Sherwood, Duke		Sherwood et al., 2004
UAS-Spastin-CFP (on III)	N. Sherwood, Duke		Du et al., 2010
fkh-Gal4 (on II)	D. Andrew (John Hopkins University)		Chung et al., 2017
fkh-Gal4 (on III)	D. Andrew (John Hopkins University)		Chung et al., 2017
ubi-Rok-GFP	S. Parkhurst (Fred Hutchinson Cancer Research Center)		Abreu-Blanco et al., 2014
sqh-GFP			Royou et al., 2004

UAS-Rab11S25N-EYFP	Bloomington Stock Center	9792, 23261	
UAS-Dicer-2	Bloomington Stock Center	60008	
UAS-Dhc64C RNAi	Bloomington Stock Center Vienna *Drosophila* Resource Center	76941, 28749, v28053, v28054. 4 lines worked equally. v28054 was used for all of the data shown in this work.	
klar^{1}	Bloomington Stock Center	3256	
klar^{mCD4}	Bloomington Stock Center	25097	
klar^{mCD4} *ubi-Rok-GFP*	Recombinant line generated from *klar*^{mCD4} and *ubi-Rok-GFP*		
UAS-Crb RNAi	Bloomington Stock Center	38373, 38903, 40869, 34999.	

		4 lines worked equally. 2 lines (38373, 34999) were used for the data shown in this work.	
UAS-Baz RNAi	Bloomington Stock Center	35002, 38213, 39072. 38213 provided the strongest phenotype and used for quantification in this work.	
UAS-E-Cad RNAi	Bloomington Stock Center	32904	
UAS-Shg-GFP	Bloomington Stock Center	58445	
UAS-Baz-GFP	Bloomington Stock Center	65845	
matα4-Gal4 (*maternal Gal4*; on II)	Bloomington Stock Center	7062	

564

565

Antibody	Source	RRID	Dilution
α-E-Cad (rat)	DSHB (deposited by T. Uemura, Kyoto University)	DCAD2 (AB_528120)	1:50
α-CrebA (rat)	Andrew lab (John Hopkins University)		1:3000
α-CrebA (rabbit)	Andrew lab (John Hopkins University)		1:5000
α-Dhc (mouse)	DSHB (deposited by J.M. Scholey, University of California)	2C11-2 (AB_2091523)	1:50
α-Rab11 (rabbit)	Andrew lab (John Hopkins University)		1:500
α-Nuf (guinea pig)	Sotillos lab (CABD)		1:500
α-acetylated α-tubulin (mouse)	Invitrogen	32-2700 (AB_2533073)	1:1000
α-tyrosinated α-tubulin (rat)	Invitrogen	MA1-80017 (AB_2210201)	1:1000
α-GFP (chick)	Invitrogen	A10262 (AB_2534023)	1:500

α-β-galactosidase (rabbit)	Invitrogen	A11132 (AB_221539)	1:500
α-Crb (mouse)	DSHB (deposited by E. Knust, Max Planck Institute)	Cq4 (AB_528181)	1:10
α-Fog (rabbit)	N. Fuse (Fuse et al., 2013)		1:1000
α-Sec15 (guinea pig)	Bellen lab (Baylor College of Medicine)		1:2000
Alexa Fluor 488/568/647-coupled secondary antibodies	Invitrogen		1:500

566

Acknowledgments

We thank the members of the Chung laboratory for comments and suggestions. We thank A. Martin, S. Parkhurst and N. Sherwood and the Bloomington stock center for fly stocks, and D. Andrew, H. Bellen, S. Sotillos and the Developmental Studies Hybridoma Bank for antibodies. We thank Flybase for the gene information. We are grateful to A. Bohnert, C. Hanlon, A. Johnson and C. O'Kane for their helpful comments on the manuscript. This work is supported by start-up fund from Louisiana State University and the grant from the Board of Regents Research Competitiveness Subprogram GR-00005224 to S.C.

576 **Figure legends**

577 **Fig. 1. Intracellular trafficking components are apically enriched near the**
578 **invagination pit.** (A) A schematic drawing of the anterior region of the *Drosophila* embryo
579 for stage 11 (ventral and lateral views) and stage 16 (lateral view). Green, SGs. Top right,
580 magnified view of a SG placode. Purple area, the region where SG cells undergo
581 clustered apical constriction during invagination. (B-D) En face (top) and lateral (bottom)
582 views of a wild type SG immunostained for E-Cad, Rab11 and Nuf. Rab11 and Nuf show
583 apical upregulation near the invagination pit (yellow arrowheads). Red arrowheads,
584 Rab11 and Nuf signals near the segmental groove. (B'-D') Heat maps of apical area (B')
585 and intensity of Rab11 and Nuf (C', D'). Cells with small apical areas (dark blue cells in
586 B') near the invagination pit show high intensity of Rab11 and Nuf (red cells in C' and D').
587 (E) Negative correlation between Rab11/Nuf intensities and apical areas of SG cells. R,
588 Pearson correlation coefficient. $p<0.0001$ for all samples (n=5 SGs; 690 cells). (F-H')
589 *Rab11-EYFP* (an EYFP insertion at the N-terminus under the control of Rab11 regulatory
590 sequences) SG labeled with antibodies against E-Cad (F), GFP (G) and Nuf (H) and
591 corresponding heat maps for apical areas (F') and intensity of GFP (G') and Nuf signals
592 (H'). Rab11-EYFP shows the same enrichment near the invagination pit (F'-H'). (I-J') En
593 face (top) and lateral (bottom) views of a wild type SG immunostained with E-Cad (I) and
594 Dhc64C (J) and corresponding heat maps for apical areas (I') and intensity of Dhc64C
595 signals (J'). Yellow arrowheads, apical upregulation of Dhc64C near the invagination pit.
596 (K-L') A *Rab7-EYFP* (an EYFP insertion at the N-terminus under the control of Rab7
597 regulatory sequences) SG immunostained with E-Cad (K) and GFP (L) and
598 corresponding heat maps for apical areas (K') and intensity of Rab7-EYFP (L'). Asterisks:
599 invagination pit. White lines: SG boundary.

Figure 1

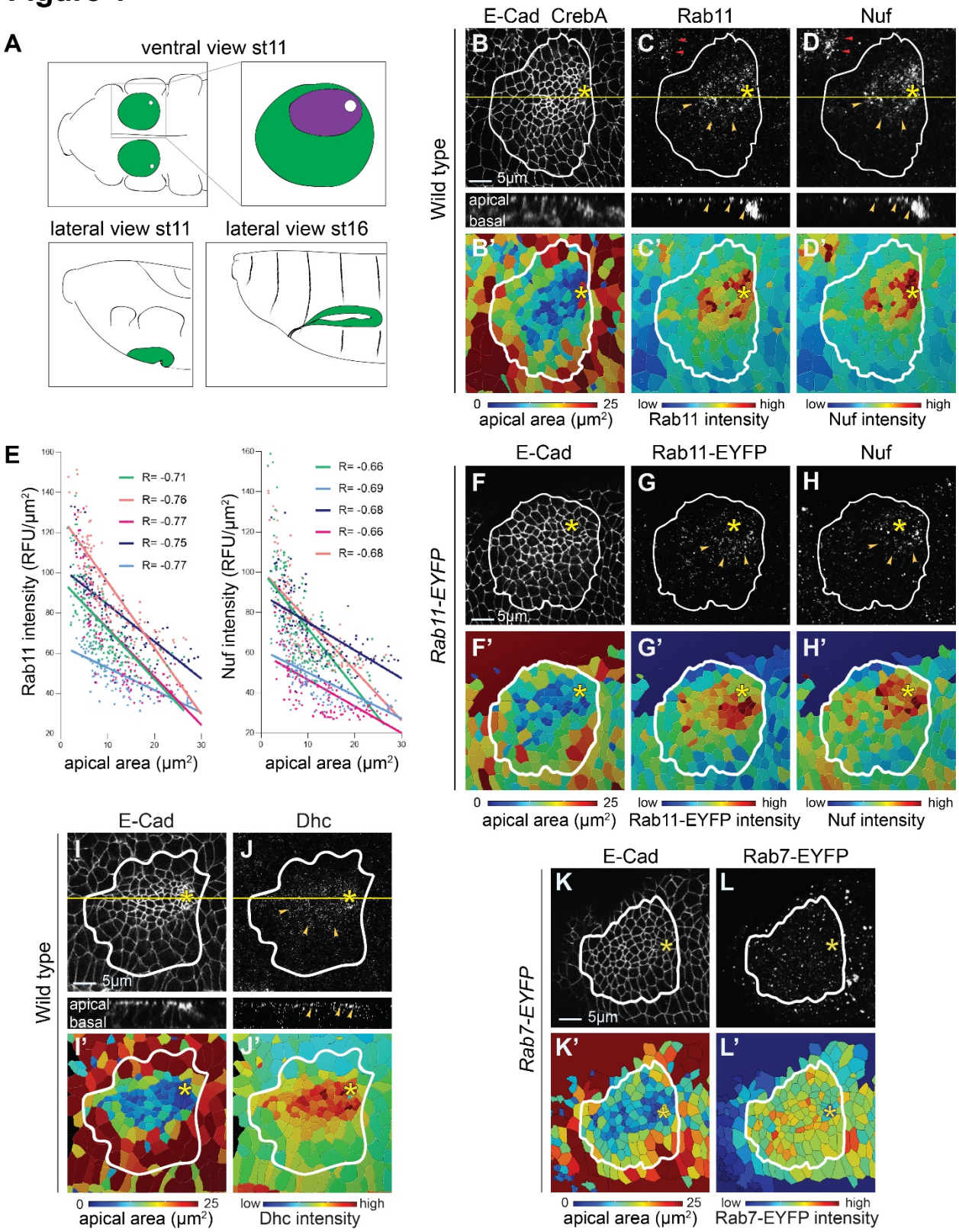
A
ventral view st11
lateral view st11
lateral view st16
E-Cad CrebA
Rab11
Nuf
Wild type
B
C
D
5µm
apical
basal
B'
C'
D'
0
25
apical area (µm²)
low
high
Rab11 intensity
Nuf intensity
E
Rab11 intensity (RFU/µm²)
Nuf intensity (RFU/µm²)
R= -0.71
R= -0.76
R= -0.77
R= -0.75
R= -0.77
R= -0.66
R= -0.69
R= -0.68
R= -0.66
R= -0.68
apical area (µm²)
E-Cad
Rab11-EYFP
Nuf
Rab11-EYFP
F
G
H
F'
G'
H'
Rab11-EYFP intensity
E-Cad
Dhc
I
J
I'
J'
Dhc intensity
E-Cad
Rab7-EYFP
Rab7-EYFP
K
L
K'
L'
Rab7-EYFP intensity

602 **Fig. 2. Disruption of MTs results in uncoordinated apical constriction, reduction of**
603 **apical vesicle numbers, and mislocalization of Rab11/Nuf.** (A-A’’’) Co-localization of
604 Rab11 and tyrosinated α-tubulin in SG cells during invagination. A wild type SG
605 immunostained with Rab11 (green) and tyrosinated α-tubulin (purple; Tyr-α-Tub) is shown
606 with higher magnification of the yellow boxed area (A’-A’’’). Yellow arrowheads, co-
607 localized Rab11 and tyrosinated α-tubulin. (B-B’’) Z sections along the yellow line in (A).
608 Yellow arrowheads, co-localized Rab11 and tyrosinated α-tubulin. (C) Thresholded
609 Manders’ colocalization coefficients show the extent to which two proteins colocalize (n=
610 6 SGs). (D-E’’’) Overexpression of spastin in the SG disrupts the MT networks and
611 compromises enrichment of Rab11 near the invagination pit. (D-D’’’) En face (top) and
612 lateral (bottom) views of a control SG show abundant levels of tyrosinated α-tubulin (D’’)
613 and acetylated α-tubulin (D’’’; Ace-α-Tub). Rab11 is enriched in the apical domain near
614 the invagination pit (yellow arrowheads). (E-E’’’) Overexpression of spastin by *fkh-Gal4*
615 leads to a loss of MTs in the SG, labelled both by tyrosinated α-tubulin (E’’) and acetylated
616 α-tubulin (E’’’). (E’) Rab11 is not enriched near the invagination pit and mislocalizes
617 basolaterally when spastin is overexpressed (red arrowheads). (F-F’’) Confocal images
618 of a spastin-overexpressing SG stained with Rab11 (F’) and Nuf (F’’) and corresponding
619 heat maps for apical areas (G), intensities of Rab11 (G’) and Nuf (G’’). Compare to control
620 SGs in Figs. 1B-H’. (H) A ratio of deviation of intensity to the median intensity of Rab11
621 (left) and Nuf (right) in all SG cells (n= 5 SGs; 690 cells). *, $p<0.01$. ****, $p<0.0001$, Mann-
622 Whitney U test. Asterisks: invagination pit. White lines: SG boundary.

Figure 2

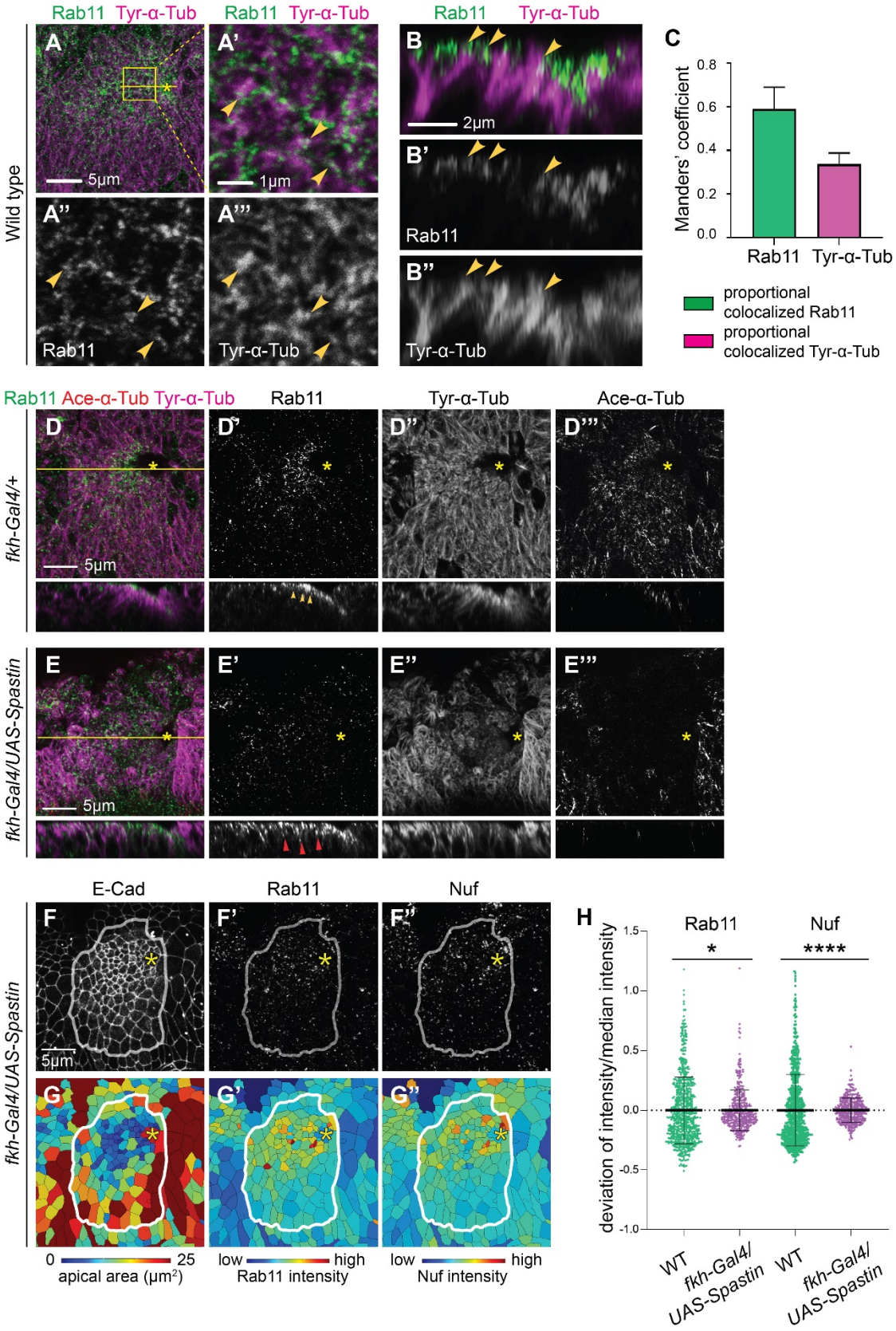
Rab11 Tyr-α-Tub
Rab11 Tyr-α-Tub
Rab11 Tyr-α-Tub
Wild type
A
A'
B
B'
B''
A''
A'''
5μm
1μm
2μm
Rab11
Tyr-α-Tub
C
Manders' coefficient
0.8
0.6
0.4
0.2
0.0
Rab11 Tyr-α-Tub
proportional colocalized Rab11
proportional colocalized Tyr-α-Tub
Rab11 Ace-α-Tub Tyr-α-Tub
Rab11
Tyr-α-Tub
Ace-α-Tub
fkh-Gal4/+
D
D'
D''
D'''
fkh-Gal4/UAS-Spastin
E
E'
E''
E'''
E-Cad
Rab11
Nuf
F
F'
F''
G
G'
G''
0 25
apical area (μm²)
low high
Rab11 intensity
low high
Nuf intensity
H
Rab11
Nuf
*
****
deviation of intensity/median intensity
1.5
1.0
0.5
0.0
-0.5
-1.0
WT
fkh-Gal4/ UAS-Spastin
WT
fkh-Gal4/ UAS-Spastin

623

624 **Fig. 3. Rab11 and the dynein motor are required for coordinated apical constriction**
625 **in the SG.** (A-C) Confocal images of control (A), Rab11-DN-overexpressing (B) and
626 *Dhc64C* RNAi (C) SGs immunostained with E-Cad. (A'-C') Heat maps corresponding to
627 images shown in A-C. (D-E') Confocal images and corresponding heat maps of wild type
628 (D, D') and *klar* mutant (E, E') SGs. (F, H) Percentage and cumulative percentage of cells
629 with different apical areas. Mann-Whitney U test (for percentage of cells) and
630 Kolmogorov-Smirnov test (for cumulative percentage of cells). n= 5 SGs (control (*fkh-*
631 *Gal4/+*), 517 cells; *Rab11-DN*, 536 cells; zygotic *Dhc64C* RNAi, 499 cells; WT, 690 cells;
632 *klar*^{1}, 705 cells; maternal/zygotic *Dhc64C* RNAi, 561 cells). **, $p<0.01$; ****, $p<0.0001$. (G)
633 A range of phenotypes is observed when *Dhc64C* is knocked down both maternally and
634 zygotically, including mild (uncoordinated apical constriction), intermediate (enlarged pit)
635 and severe (deformed epithelial tissue and additional folds) phenotypes. Asterisks:
636 invagination pit. White lines: SG boundary. (H) Percentage and cumulative percentage of
637 cells with different areas in SGs that were knocked down *Dhc64C* both maternally and
638 zygotically.

Figure 3

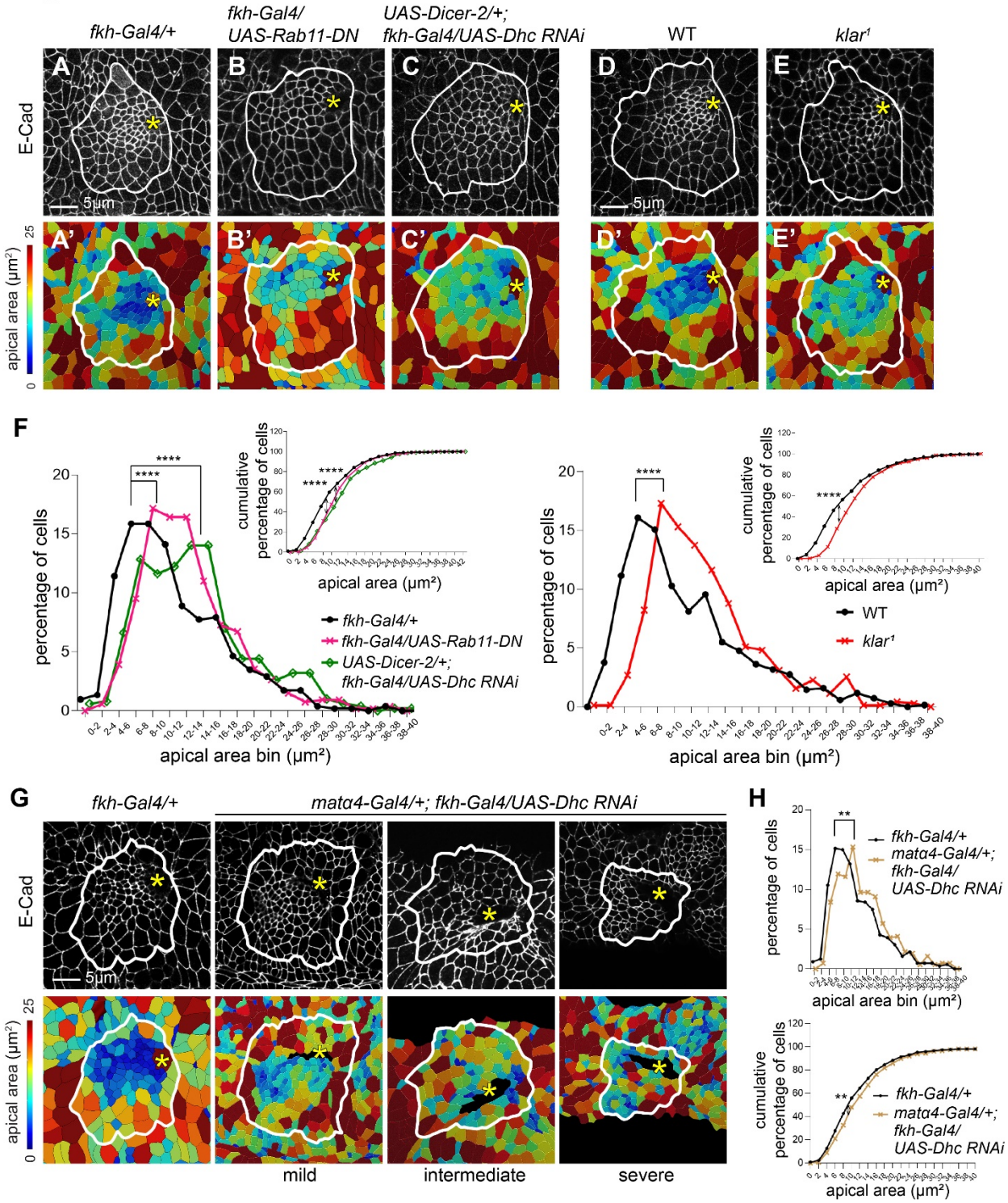
fkh-Gal4/+
fkh-Gal4/ UAS-Rab11-DN
UAS-Dicer-2/+; fkh-Gal4/UAS-Dhc RNAi
WT
klar¹
E-Cad
5µm
apical area (µm²)
F
percentage of cells
cumulative percentage of cells
apical area (µm²)
apical area bin (µm²)
fkh-Gal4/+
fkh-Gal4/UAS-Rab11-DN
UAS-Dicer-2/+; fkh-Gal4/UAS-Dhc RNAi
WT
klar¹
G
fkh-Gal4/+
matα4-Gal4/+; fkh-Gal4/UAS-Dhc RNAi
mild
intermediate
severe
H
fkh-Gal4/+
matα4-Gal4/+; fkh-Gal4/ UAS-Dhc RNAi

643 **Fig. 4. Compromised intracellular trafficking leads to a reduction of apicomedial**
644 **myosin formation in the SG cells.** (A-B’’’’) sqh-GFP signals in control (A-A’’’’) and
645 *Dhc64C* RNAi (B-B’’’’) SGs. (A’’-B’’’’) Higher magnification of the yellow boxed area in A
646 and B. *Dhc64C* knockdown leads to reduced apicomedial myosin (red arrowheads in B’’)
647 compared to strong signals of apicomedial myosin in A’’ (yellow arrowheads). (C)
648 Quantification of apicomedial myosin, junctional myosin and the ratio of apicomedial to
649 junctional myosin in *Dhc64C* RNAi SG cells. (D-E’’’’) Myosin signals in control (D-D’’’’)
650 and in *klar* mutant (E-E’’’’) SGs. (D’’-E’’’’) Higher magnification of the yellow boxed area
651 in D and E. *Dhc64C* knockdown leads to reduced apicomedial myosin (red arrowheads
652 in E’’); compare these to strong signals of apicomedial myosin in D’’ (yellow arrowheads).
653 (F) Quantification of apicomedial myosin, junctional myosin and the ratio of apicomedial
654 to junctional myosin in control and *klar* mutant SG cells. n= 5 SGs for all genotypes; 10
655 cells in the dorsal/posterior region of each SG. *, $p< 0.05$. **, $p< 0.01$. ***, $p< 0.001$. ****,
656 $p<0.0001$, Mann-Whitney U test. Asterisks: invagination pit.

Figure 4

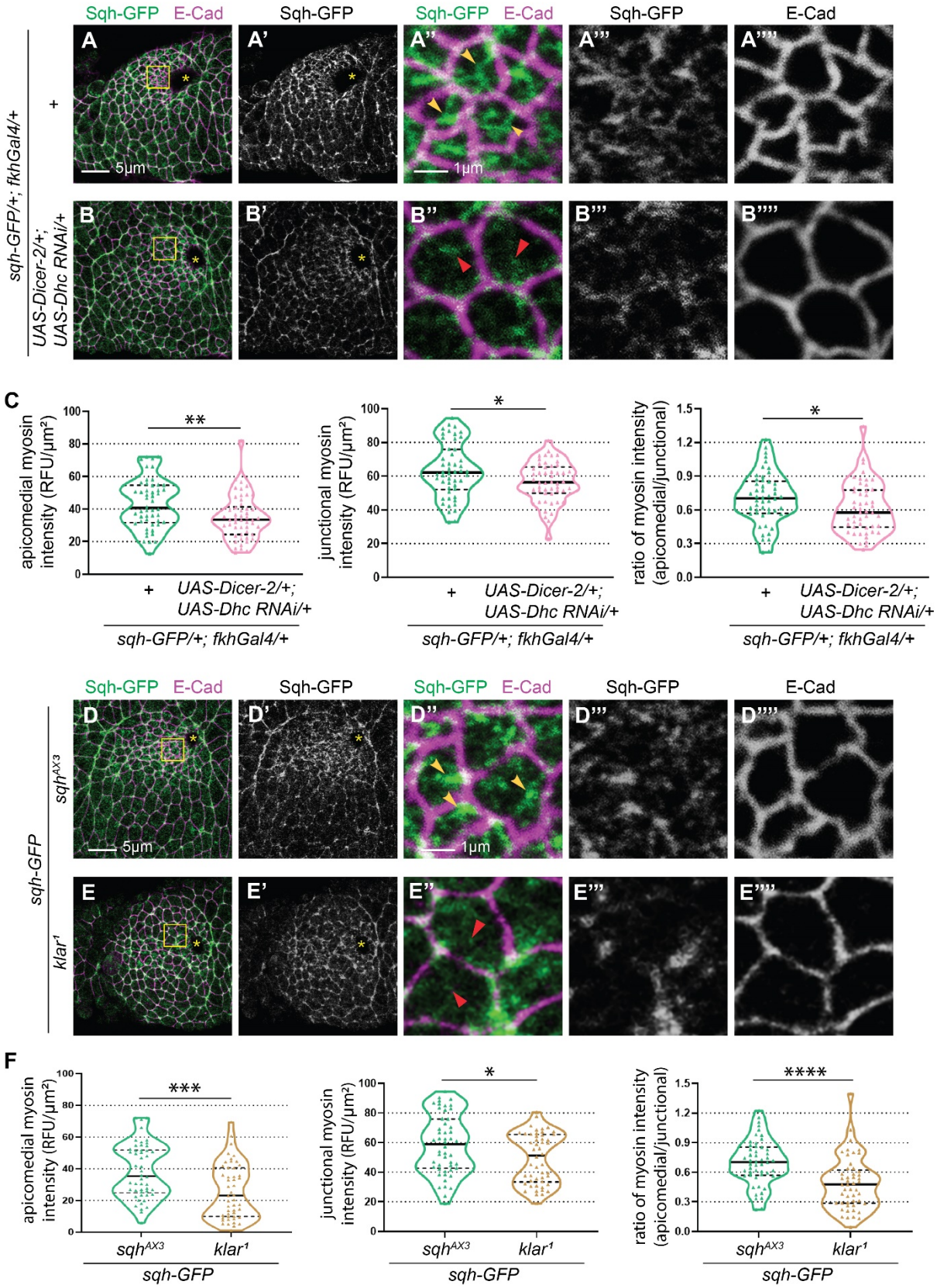
Sqh-GFP E-Cad
Sqh-GFP
Sqh-GFP E-Cad
Sqh-GFP
E-Cad
A
A'
A''
A'''
A''''
B
B'
B''
B'''
B''''
5µm
1µm
sqh-GFP/+; fkhGal4/+
+
UAS-Dicer-2/+; UAS-Dhc RNAi/+
C
apicomedial myosin intensity (RFU/µm²)
junctional myosin intensity (RFU/µm²)
ratio of myosin intensity (apicomedial/junctional)
**
*
*
+
UAS-Dicer-2/+; UAS-Dhc RNAi/+
sqh-GFP/+; fkhGal4/+
D
D'
D''
D'''
D''''
E
E'
E''
E'''
E''''
sqh-GFP
sqhAX3
klar1
F
***
*
****
sqhAX3
klar1
sqh-GFP

658 **Fig. 5. Compromised MT-based intracellular trafficking impairs accumulation of**
659 **apicomedial Rok within constricting cells during invagination.** (A-A'') A control SG
660 shows accumulation of Rok-GFP signals (green) in the apicomedial region of cells near
661 the invagination pit. E-Cad (magenta), cell boundary. Yellow arrowheads, accumulative
662 Rok-GFP. (B-C'') Rok-GFP signals are more dispersed in SG cells upon spastin
663 overexpression (B-B'') and knockdown of *Dhc64C* (C-C'') (red arrowheads). (D) A control
664 SG homozygous for ubi-Rok-GFP shows a huge accumulation of Rok-GFP in constricting
665 cells (yellow arrowheads). (E) A mutation in *klar* results in slightly reduced accumulation
666 of Rok-GFP in cells near the invagination pit (red arrowheads). (F) Representative images
667 for how areas of Rok-GFP puncta were measured using the Fiji software. (G,H)
668 Quantification of areas of Rok-GFP puncta. ****, $p < 0.0001$, Mann-Whitney U test. n= 5
669 SGs for all genotypes; 15 cells in the dorsal/posterior region for each SG.
670

Figure 5

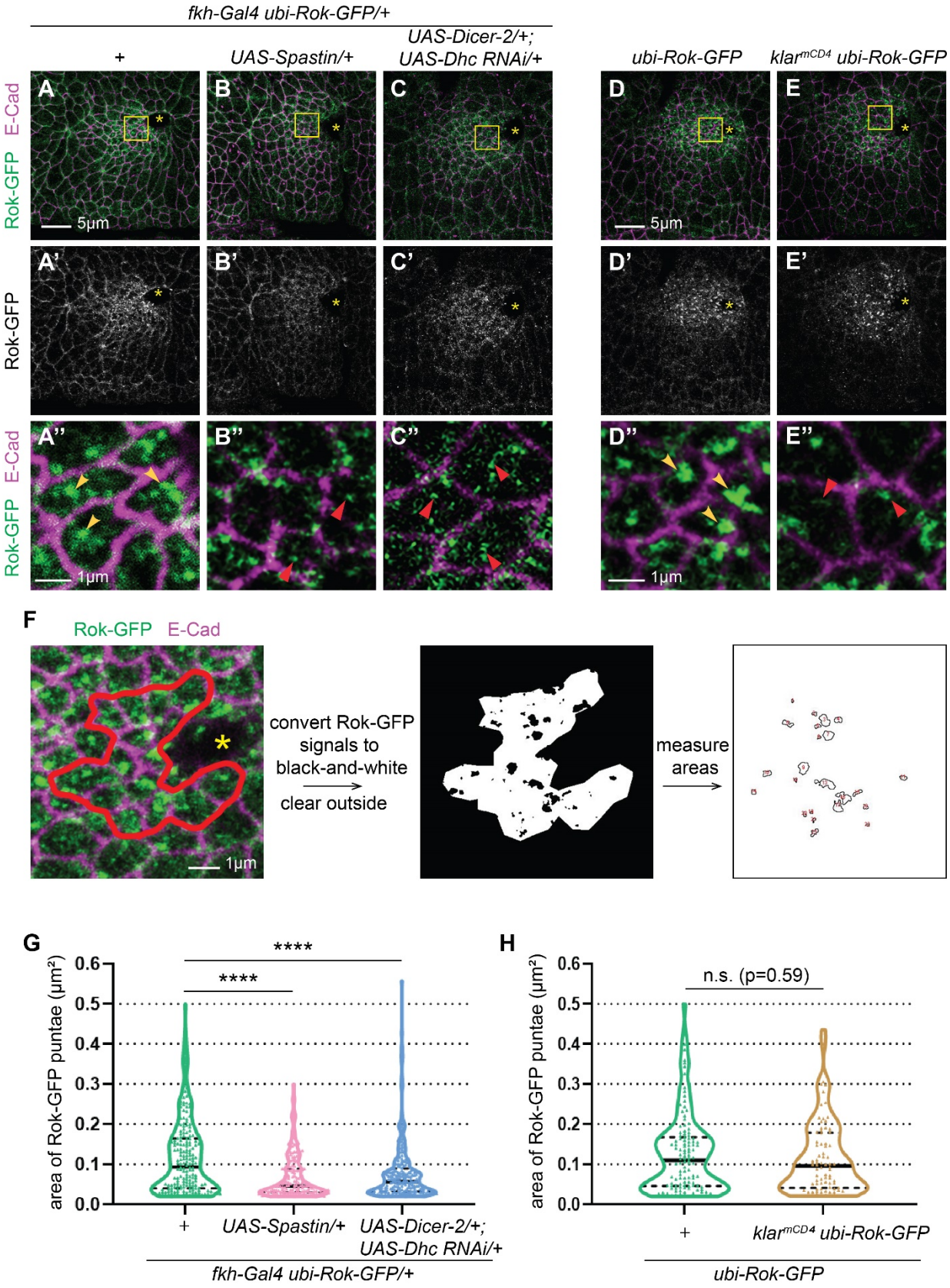
fkh-Gal4 ubi-Rok-GFP/+
+
UAS-Spastin/+
UAS-Dicer-2/+; UAS-Dhc RNAi/+
ubi-Rok-GFP
klarmCD4 ubi-Rok-GFP
Rok-GFP E-Cad
Rok-GFP
Rok-GFP E-Cad
5µm
1µm
F
Rok-GFP E-Cad
convert Rok-GFP signals to black-and-white
clear outside
measure areas
G
area of Rok-GFP puntae (µm²)
****
****
+
UAS-Spastin/+
UAS-Dicer-2/+; UAS-Dhc RNAi/+
fkh-Gal4 ubi-Rok-GFP/+
H
n.s. (p=0.59)
klarmCD4 ubi-Rok-GFP
ubi-Rok-GFP

671

672 **Fig. 6. Impairing microtubule-based trafficking suppresses the over-active Fog**
673 **signaling pathway.** (A-A') Rok-GFP signals in constricting cells in a control SG (yellow
674 arrowheads). (B-B') In Fog-overexpressing SGs, Rok-GFP is over-accumulated in cells
675 (red arrowheads). (C-D') The Rok over-accumulation phenotype is suppressed when
676 spastin is overexpressed or *Dhc64C* is knocked down (red arrows). (E-E') Apicomedial
677 myosin in the control SG (yellow arrowheads). (F-F') Fog-overexpressing SG cells show
678 increased apicomedial myosin (red arrowheads). (G-H') Upregulation of apicomedial
679 myosin caused by Fog overexpression is inhibited when spastin is overexpressed or
680 *Dhc64C* is knocked down (red arrows). (I-I') Fog overexpressing SG cells show wavy
681 adherens junctions (E-Cad) signals. Cell junctions are deformed at the contact sites to
682 apicomedial myosin (red arrowheads). (J) Quantification of areas of Rok-GFP puncta. (n=
683 5 SGs; 15 cells for each SG). (K) Left, a cartoon for how the tortuosity of a cell junction
684 was measured. Right, quantification of the tortuosity (n= 5 SGs; 10 cells for each SG;
685 ~280 junctions). (L) Quantification of apicomedial myosin, junctional myosin and the ratio
686 of apicomedial to junctional myosin (n= 5 SGs; 10 cells for each SG). For all quantification,
687 cells in the dorsal/posterior region of SG placode were used. *, $p< 0.05$. **, $p< 0.01$. ***,
688 $p< 0.001$. ****, $p< 0.0001$, Mann-Whitney U test. Asterisks: invagination pit.

Figure 6

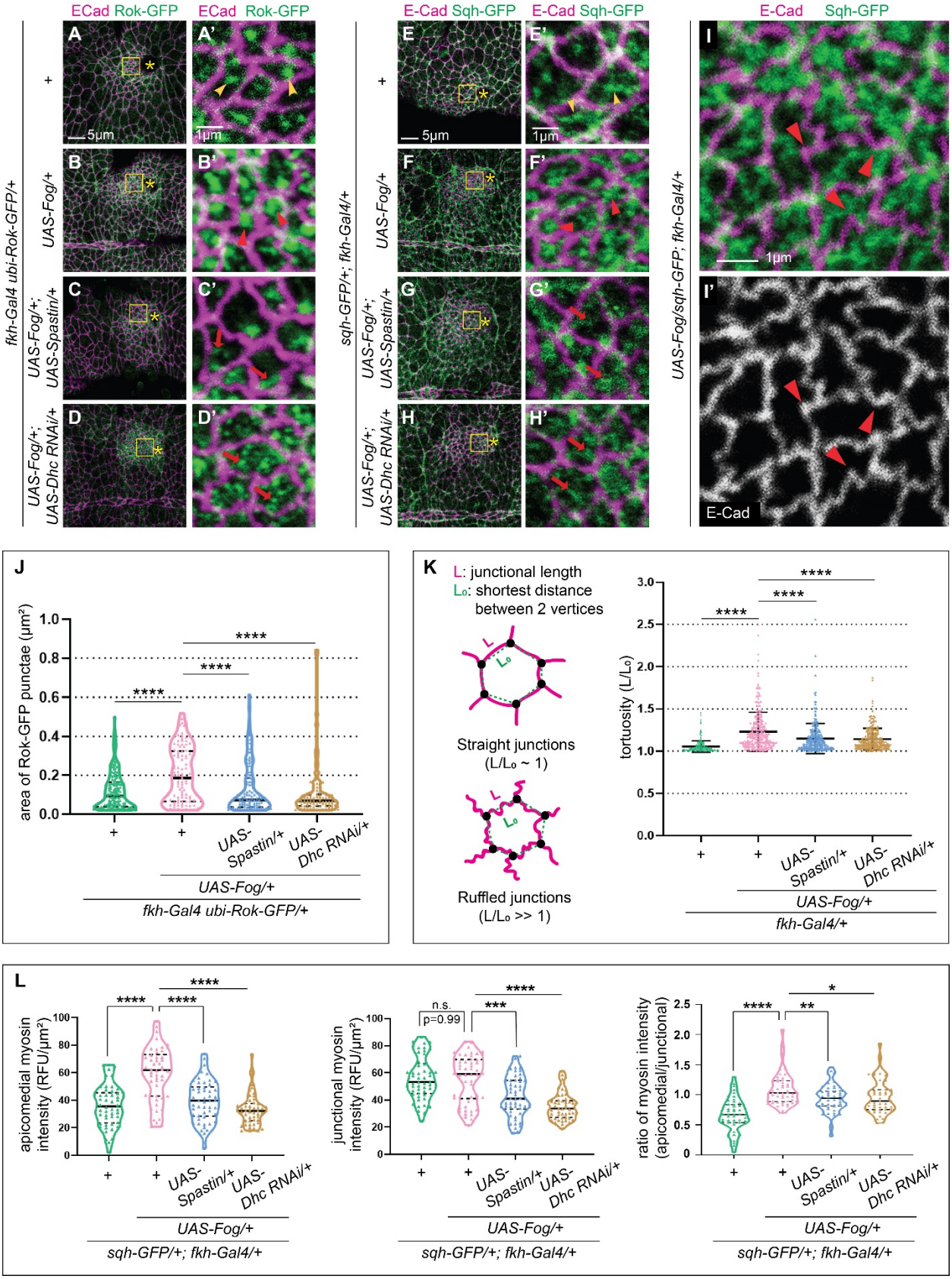
ECad Rok-GFP
ECad Rok-GFP
E-Cad Sqh-GFP
E-Cad Sqh-GFP
E-Cad
Sqh-GFP
fkh-Gal4 ubi-Rok-GFP/+
+
UAS-Fog/+
UAS-Fog/+; UAS-Spastin/+
UAS-Fog/+; UAS-Dhc RNAi/+
sqh-GFP/+; fkh-Gal4/+
UAS-Fog/sqh-GFP; fkh-Gal4/+
5µm
1µm
E-Cad
J
area of Rok-GFP punctae (µm²)
UAS-Spastin/+
UAS-Dhc RNAi/+
UAS-Fog/+
fkh-Gal4 ubi-Rok-GFP/+
K
L: junctional length
L₀: shortest distance between 2 vertices
Straight junctions (L/L₀ ~ 1)
Ruffled junctions (L/L₀ >> 1)
tortuosity (L/L₀)
fkh-Gal4/+
L
apicomedial myosin intensity (RFU/µm²)
junctional myosin intensity (RFU/µm²)
ratio of myosin intensity (apicomedial/junctional)
n.s.
p=0.99
sqh-GFP/+; fkh-Gal4/+

689

690 **Fig. 7. Crb, E-Cad and Baz have a role in regulating apical constriction during SG**
691 **invagination.** (A-B'') Control and spastin-overexpressing SGs immunostained with E-
692 Cad and Crb. (C-D') Higher magnification of boxed areas in A' and B'. Crb staining shows
693 gaps along the junctions in spastin-overexpressing SGs (yellow arrows). (E,F) Control
694 and spastin-overexpressing SGs immunostained with Baz. (G-I) Quantification of
695 junctional signals for Crb (G), E-Cad (H) and Baz (I). n= 3 SGs; 30 cells for each SG. (J,
696 K) Quantification of the ratio of length of gaps to junctional length (J; Mann-Whitney U
697 test) and the number of gaps (K; Student t-test) in SGs immunostained with Crb. n= 4
698 SGs; 10 cells for each SG. (L-O') Confocal images of SGs stained with E-Cad (L-O) and
699 corresponding heat maps for apical areas (L'-O'). (H) Percentage and cumulative
700 percentage of cells with different apical areas. Mann-Whitney U test (percentage of cells)
701 and Kolmogorov-Smirnov test (cumulative percentage of cells). n= 5 SGs (control, 517
702 cells; *crb* RNAi, 583 cells; *E-Cad* RNAi, 712 cells; *baz* RNAi, 601 cells). *, $p<0.05$. **,
703 $p<0.01$, ****, $p<0.0001$. Asterisks: invagination pit.

704

Figure 7

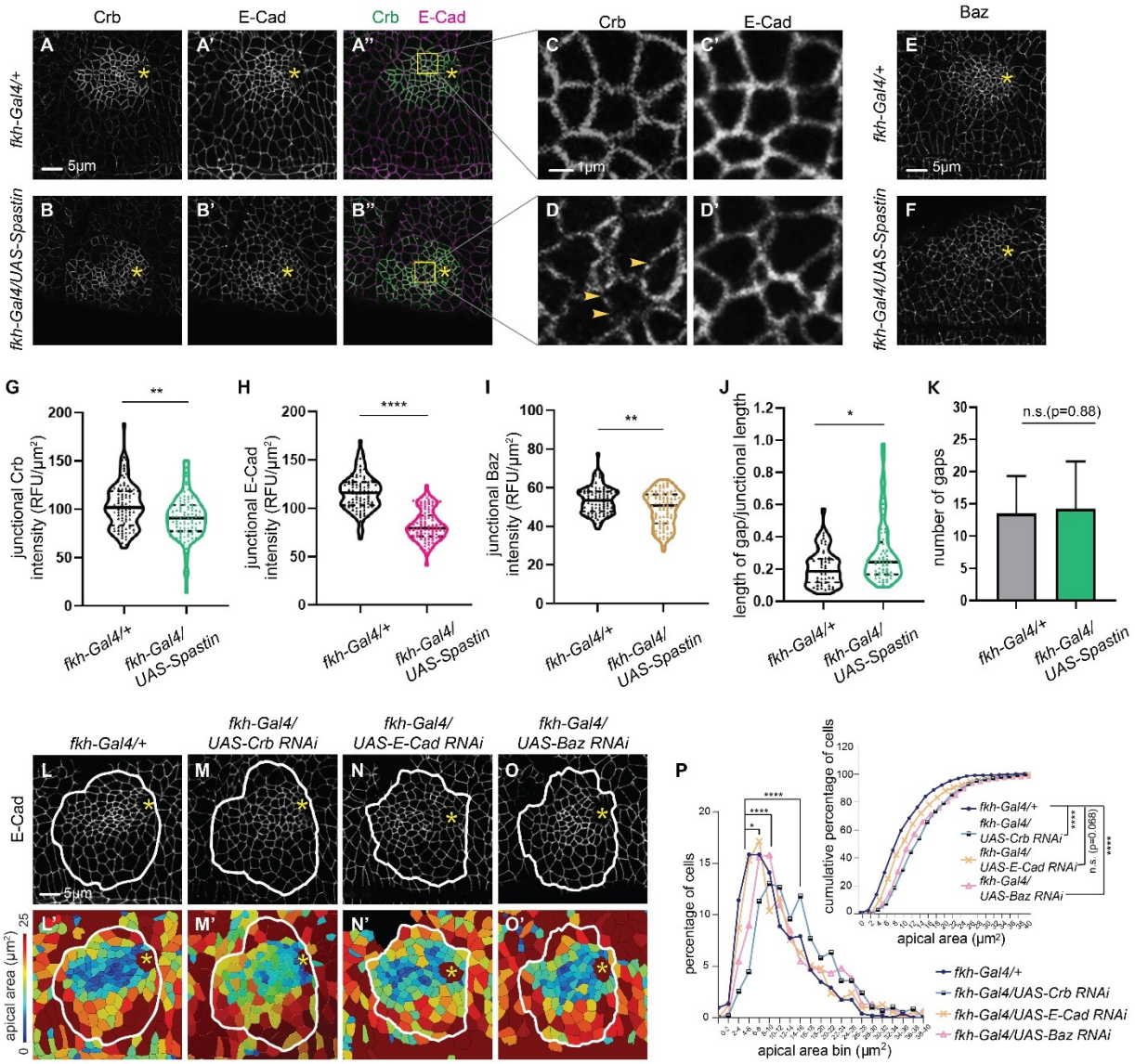

705

706

707 **Fig. 8. Knockdown of *crb*, *E-Cad* or *baz* results in reduced apicomedial myosin**
708 **formation and dispersed apicomedial Rok.** (A-D”) Compared to strong apicomedial
709 myosin in control SGs (yellow arrowheads in A’’), knockdown of *crb*, *E-Cad* or *baz* results
710 in reduction of apicomedial myosin in SG cells near the invagination pit (red arrowheads
711 in B’’-D’’). (A”-D”) Higher magnification of yellow boxed areas shown in A-D. (E)
712 Quantification of apicomedial myosin, junctional myosin and ratio of apicomedial to
713 junctional myosin of SG cells from different genotypes shown in A-D (n=5 SGs for each
714 genotype; 10 cells in the dorsal/ posterior region). **, p<0.01. ***, p< 0.001. ****, p<0.0001.
715 Mann-Whitney U test. (F-I’’) Compared to Rok accumulation in control SGs (yellow
716 arrowheads in F’’), reduction of *crb*, *E-Cad* or *baz* causes less accumulating Rok-GFP
717 signals in the apical domain of cells near the pit (red arrowheads in G’’-I’’). (F’’-I’’) Higher
718 magnification of yellow boxed areas shown in F-I. (J) Quantification of areas of Rok-GFP
719 puncta in SG cells from different genotypes shown in F-I (n=5 SGs; 15 cells in the
720 dorsal/posterior for each genotype). **, p< 0.01. ****, p< 0.0001. Mann-Whitney U test.
721 Asterisks: invagination pit.

Figure 8

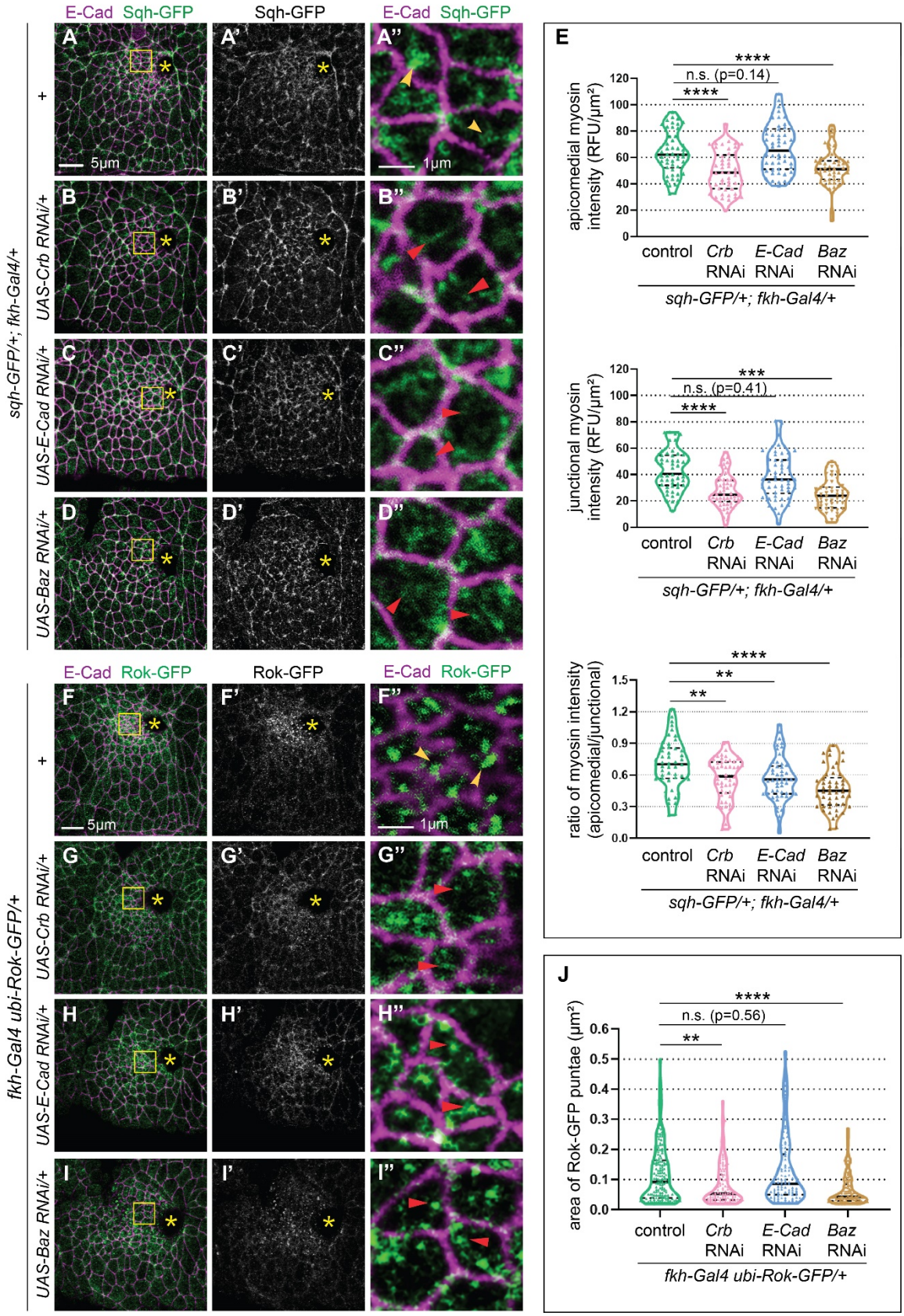
E-Cad Sqh-GFP
Sqh-GFP
E-Cad Sqh-GFP
A
A'
A''
5µm
1µm
B
B'
B''
C
C'
C''
D
D'
D''
+
UAS-Crb RNAi/+
UAS-E-Cad RNAi/+
UAS-Baz RNAi/+
sqh-GFP/+; fkh-Gal4/+
E-Cad Rok-GFP
Rok-GFP
E-Cad Rok-GFP
F
F'
F''
G
G'
G''
H
H'
H''
I
I'
I''
fkh-Gal4 ubi-Rok-GFP/+
E
apicomedial myosin intensity (RFU/µm²)
****
n.s. (p=0.14)
****
control
Crb RNAi
E-Cad RNAi
Baz RNAi
sqh-GFP/+; fkh-Gal4/+
junctional myosin intensity (RFU/µm²)
***
n.s. (p=0.41)
****
ratio of myosin intensity (apicomedial/junctional)
****
**
**
J
area of Rok-GFP puntae (µm²)
****
n.s. (p=0.56)
**
fkh-Gal4 ubi-Rok-GFP/+

722

723 **Fig. 9. A proposed model for MT-dependent trafficking to promote apical**
724 **constriction during SG invagination.** Vesicular transport is essential for apical
725 localization of Crb, E-Cad, and Baz to regulate apical myosin networks and subsequent
726 apical constriction. Fog signaling activity also depends on MTs and dynein motors.

727

728

729

Figure 9

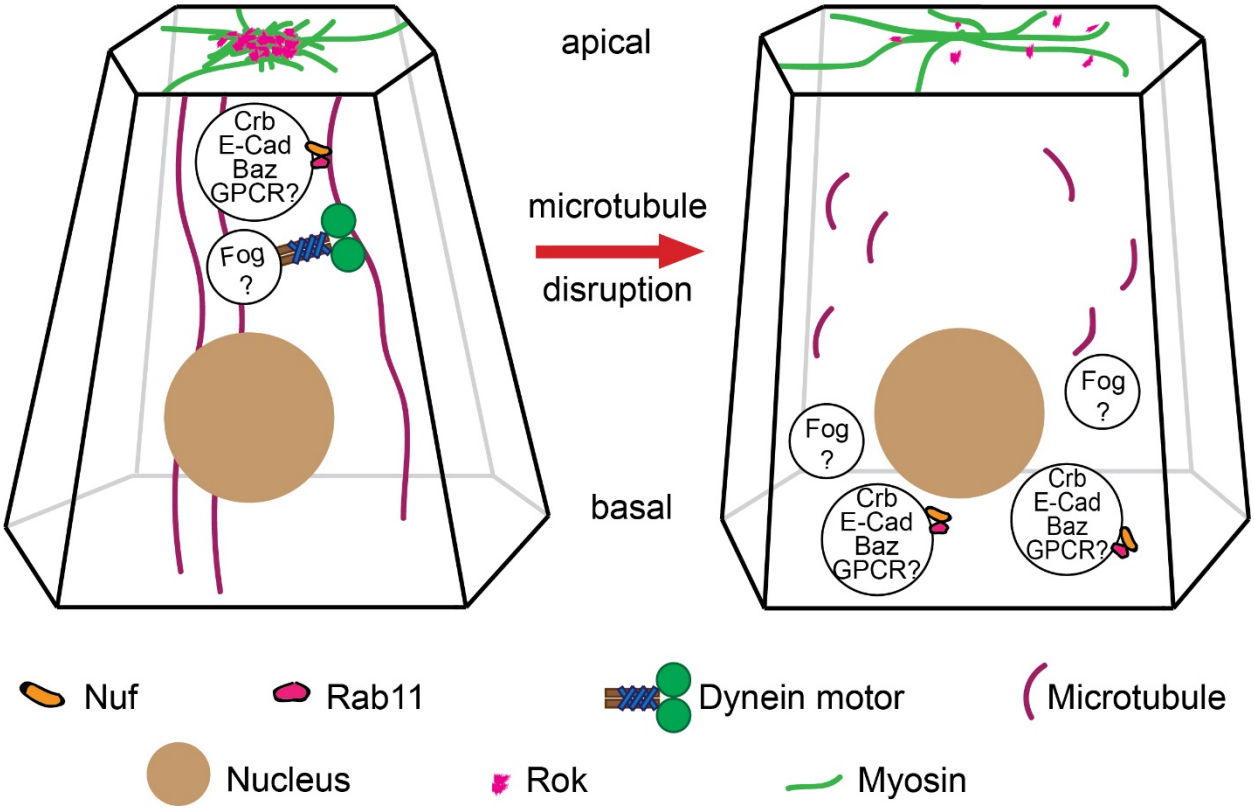

730

731

732 **Supplemental Fig. 1. Sec15 and Rab5-EYFP are enriched near the invagination pit**
733 **during SG invagination.** (A-B') Confocal images of a Rab5-EYFP SG stained with E-
734 Cad (A) and GFP (B). Rab5-EYFP is an EYFP insertion at the N-terminus under the
735 control of Rab5 regulatory sequences. GFP signals are upregulated in the apical region
736 near the invagination pit. (A', B') Heat maps of apical areas (A') and intensity of Rab5-
737 EYFP signals (B'). Cells with small apical areas (dark blue cells in A') near the
738 invagination pit show high intensity of Rab5-EYFP (red cells in B'). (C) Negative
739 correlation between Rab5-EYFP intensity and apical areas of SG cells (n= 4 SGs; 396
740 cells). (D-E') Sec15 is upregulated in the cells near the invagination pit. (D, E) Wild type
741 embryo immunostained with E-Cad and Sec15. (D', E') Heat maps of apical areas (D')
742 and intensity of Sec15 signals (E'). (F) Negative correlation between intensity of Sec15
743 and apical areas of SG cells (n= 5 SGs; 527 cells). Asterisks: invagination pit.

Supplemental Figure 1

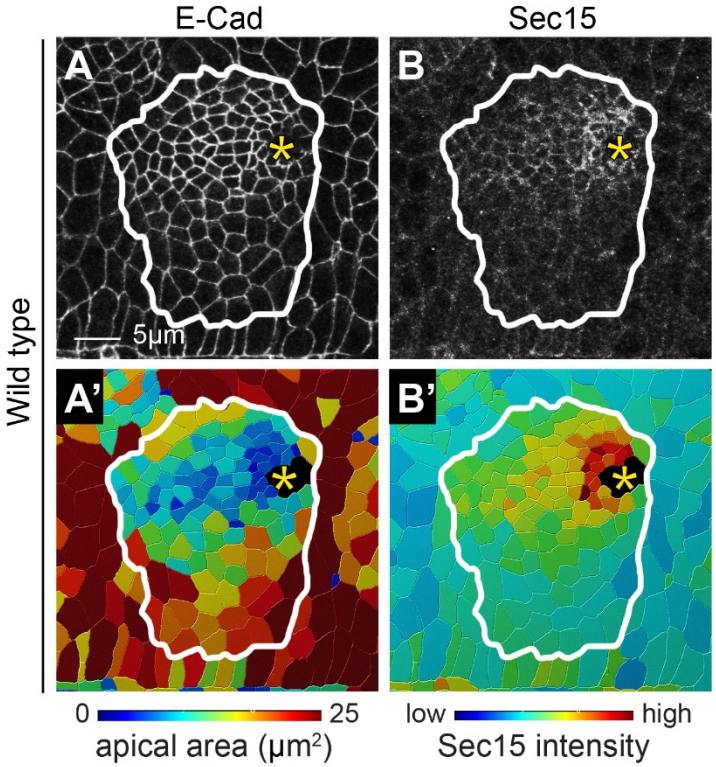

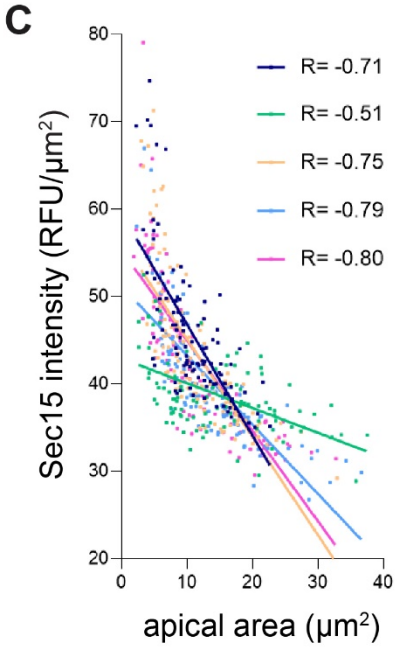

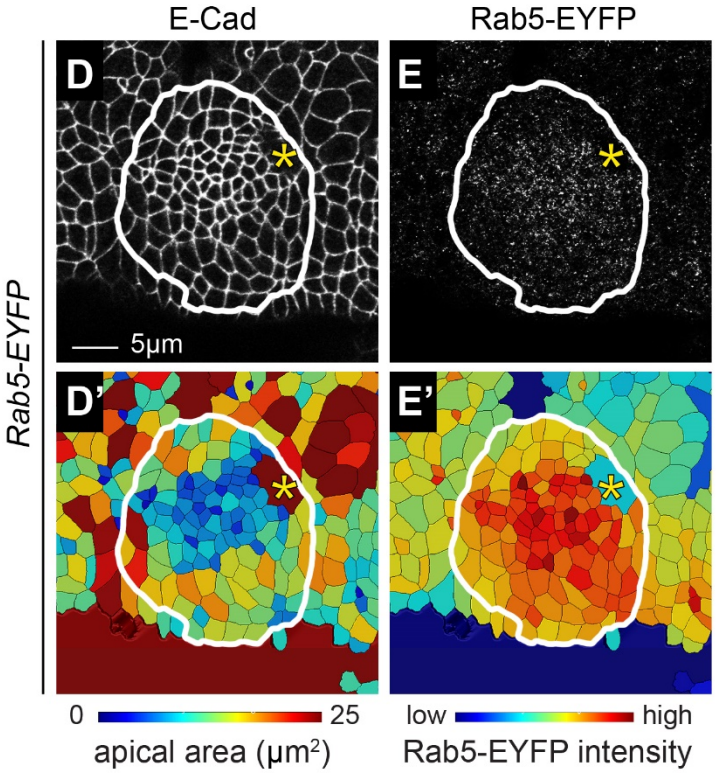

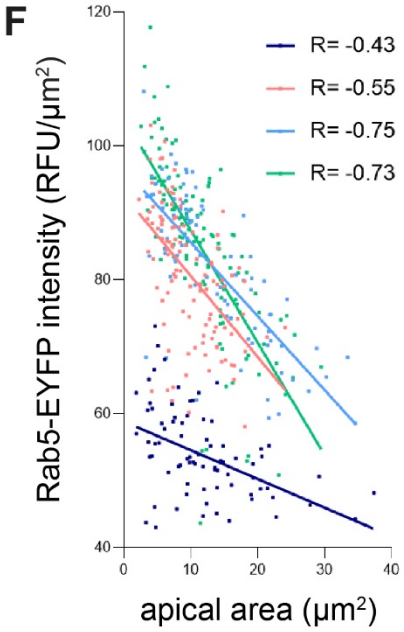

744

745 **Supplemental Fig. 2. Overexpression of spastin results in loss of acetylated-α-**
746 **tubulin in SG cells.** (A-B'') Confocal images of a control (A-A'') and spastin-CFP-
747 overexpressing SG (B-B'') stained with phalloidin (red) and acetylated α-tubulin
748 (magenta). Spastin-CFP (green) signals show SG-specific overexpression of spastin by
749 fkh-Gal4, which leads to a loss of MTs in that region. Asterisks, invagination pit.

750

751

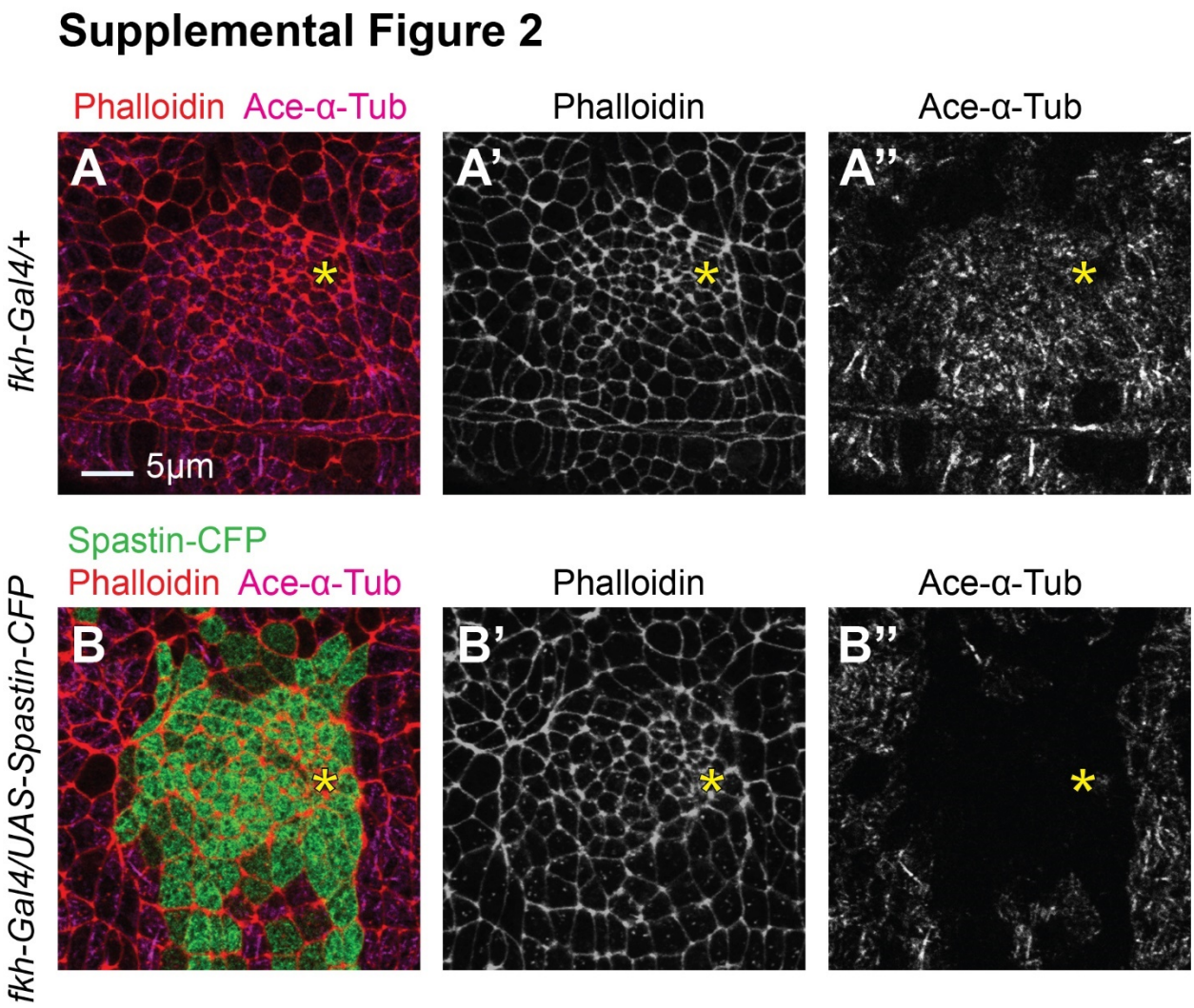

752
753

754 **Supplemental Fig. 3. Knockdown of *crb*, *E-Cad* and *baz* reduces Crb, E-Cad and**
755 **Baz levels in the SG.** (A-C'') Compared to strong Crb, E-Cad and Baz signals in control
756 SGs (A-C), knockdown of *crb*, *E-Cad* and *baz* results in reduction of Crb, E-Cad and Baz
757 levels in SG cells near the invagination pit (A'-C'). (A''-C'') Quantification of junctional
758 intensity of Crb, E-Cad and Baz. n=5 SGs (10 cells in the dorsal/posterior region of each
759 SG were tested). ****, $p < 0.0001$ (Mann-Whitney U test). Asterisks, invagination pit.

760

Supplemental Figure 3

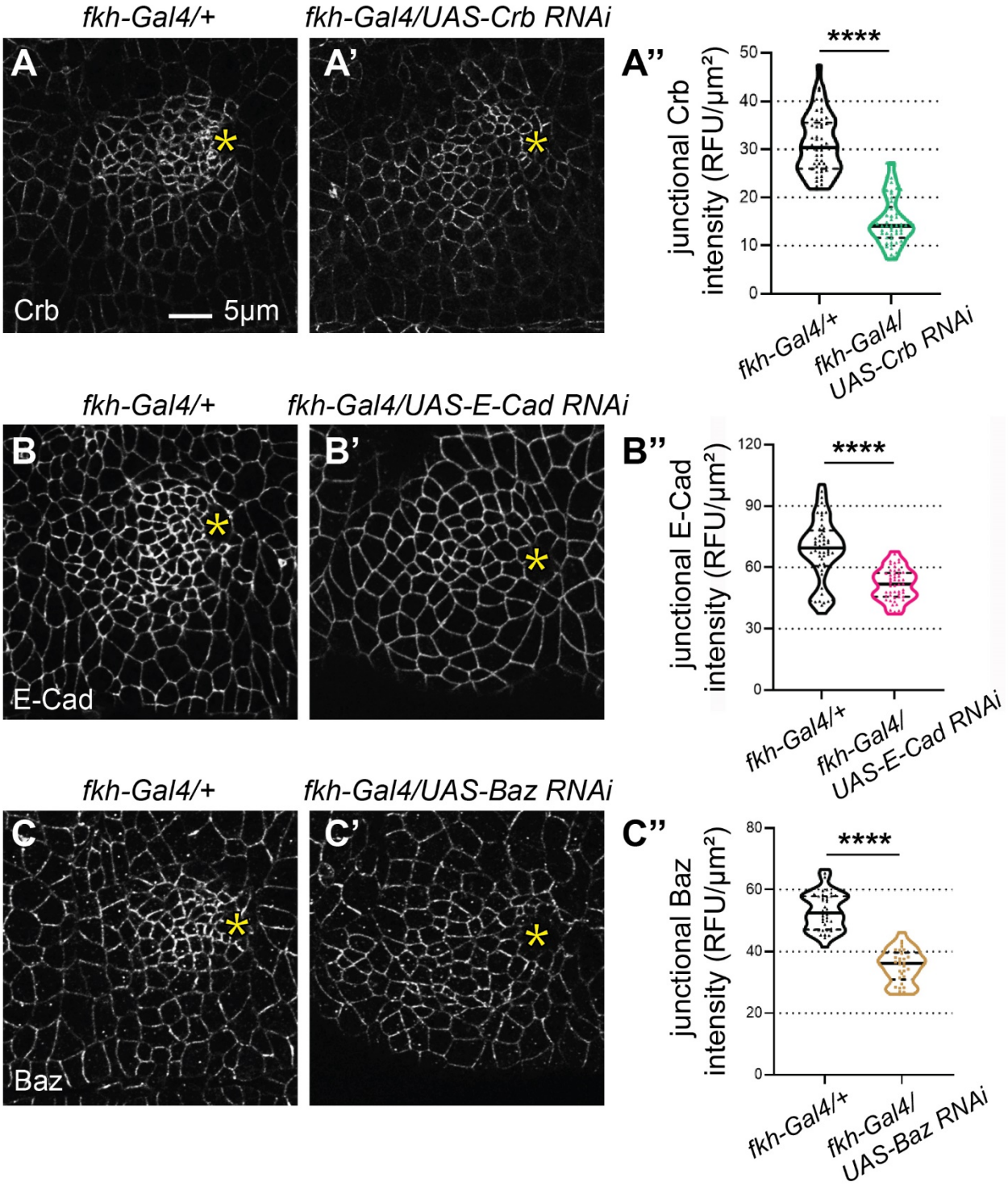

761

762 **Supplemental Fig. 4. Disruption of MTs reduces Crb levels on the apical surface in**
763 **Crb-overexpressing SG cells.** (A-C) Stage 11 SGs immunostained with Crb. (A'-C')
764 Higher magnification of the yellow boxed areas in A-C. Compared to control (A, A'),
765 overexpression of Crb (B, B') results in accumulation of Crb on the cell surface (yellow
766 arrowheads). (C-C') Co-overexpression of spastin and Crb suppresses accumulation of
767 Crb.
768

Supplemental Figure 4

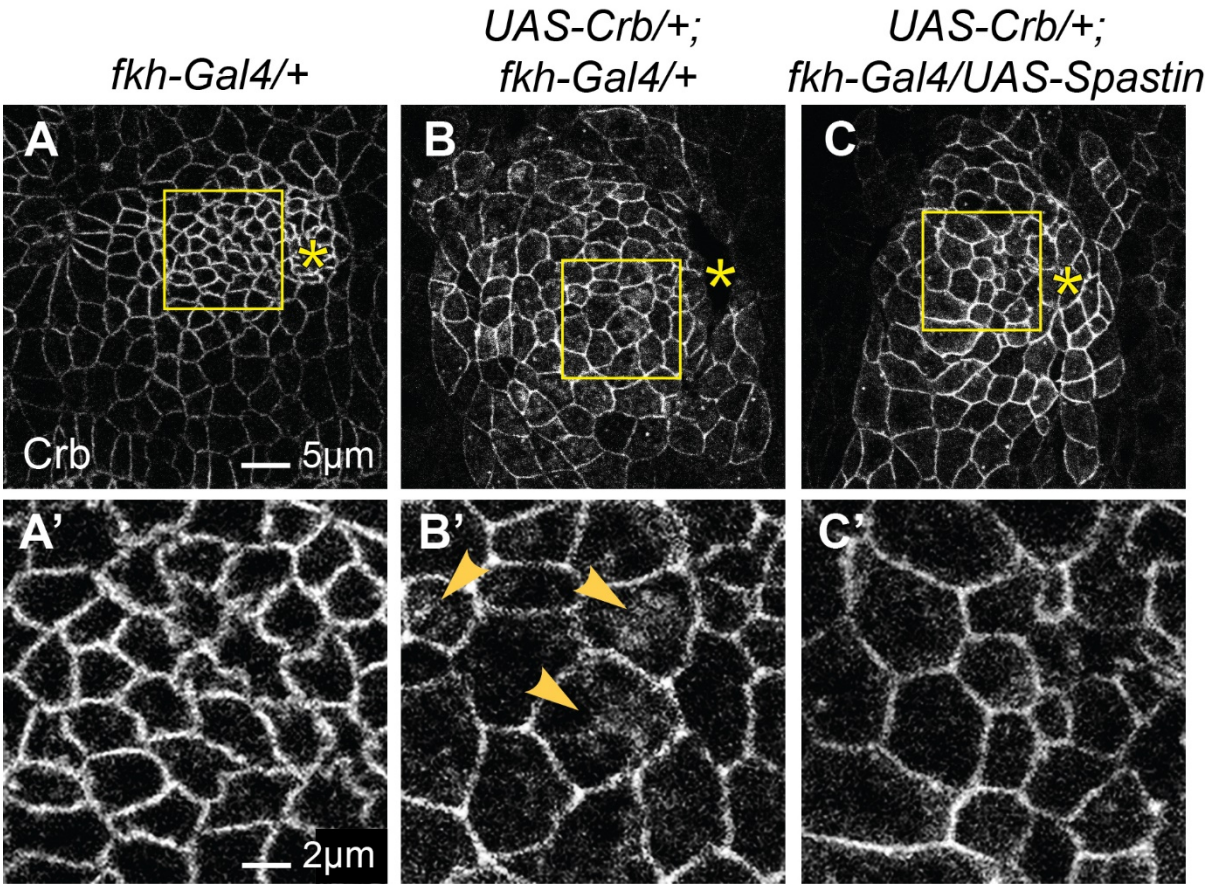

769

770

771 **Supplemental Fig. 5. MTs play a role in trafficking key apical and junctional proteins**
772 **during SG formation.** (A-B"') Overexpression of spastin results in mislocalization of
773 Rab11 and Nuf in stage 16 SGs. (A-A''') In control, Rab11 and Nuf localize in the apical
774 region of SG cells (red arrowheads). (B-B''') In spastin-overexpressing SGs, Rab11 and
775 Nuf are mislocalized to aggregates in the cytoplasm of cells (yellow arrowheads). (C-C''')
776 Overexpression of Crb causes mislocalization of Crb in all membrane domains and
777 expands the membrane. Rab11 is still enriched in the apical domain (red arrowheads).
778 (D-D''') Co-overexpression of spastin and Crb results in mislocalization of Crb to large
779 aggregates in the cytoplasm, which overlap with Rab11 (yellow arrowheads). (E-E''')
780 Overexpression of E-Cad causes a slight increase of the apical membrane, with the
781 majority of E-Cad signals in the apical domain (red arrowheads) and only some punctate
782 E-Cad signals in the basolateral region (blue arrows). (F-F''') Co-overexpression of E-
783 Cad and spastin causes mislocalization of E-Cad to cytoplasmic aggregates, which
784 overlap with Nuf (yellow arrowheads). (G-G''') Overexpression of Baz causes a slightly
785 enlarged lumen. Red arrowheads, apical localization of Baz and Nuf. (H-H''') The
786 enlarged lumen phenotype caused by Baz overexpression is suppressed when spastin is
787 co-overexpressed. Blue arrows, a pool of mislocalized Nuf overlaps with mislocalized
788 Baz. Yellow arrowheads, mislocalized Nuf that does not overlap with Baz. White dashed
789 line, cell and nuclear boundaries (H) and apical membrane (I). Nu, nucleus.
790

Supplemental Figure 5

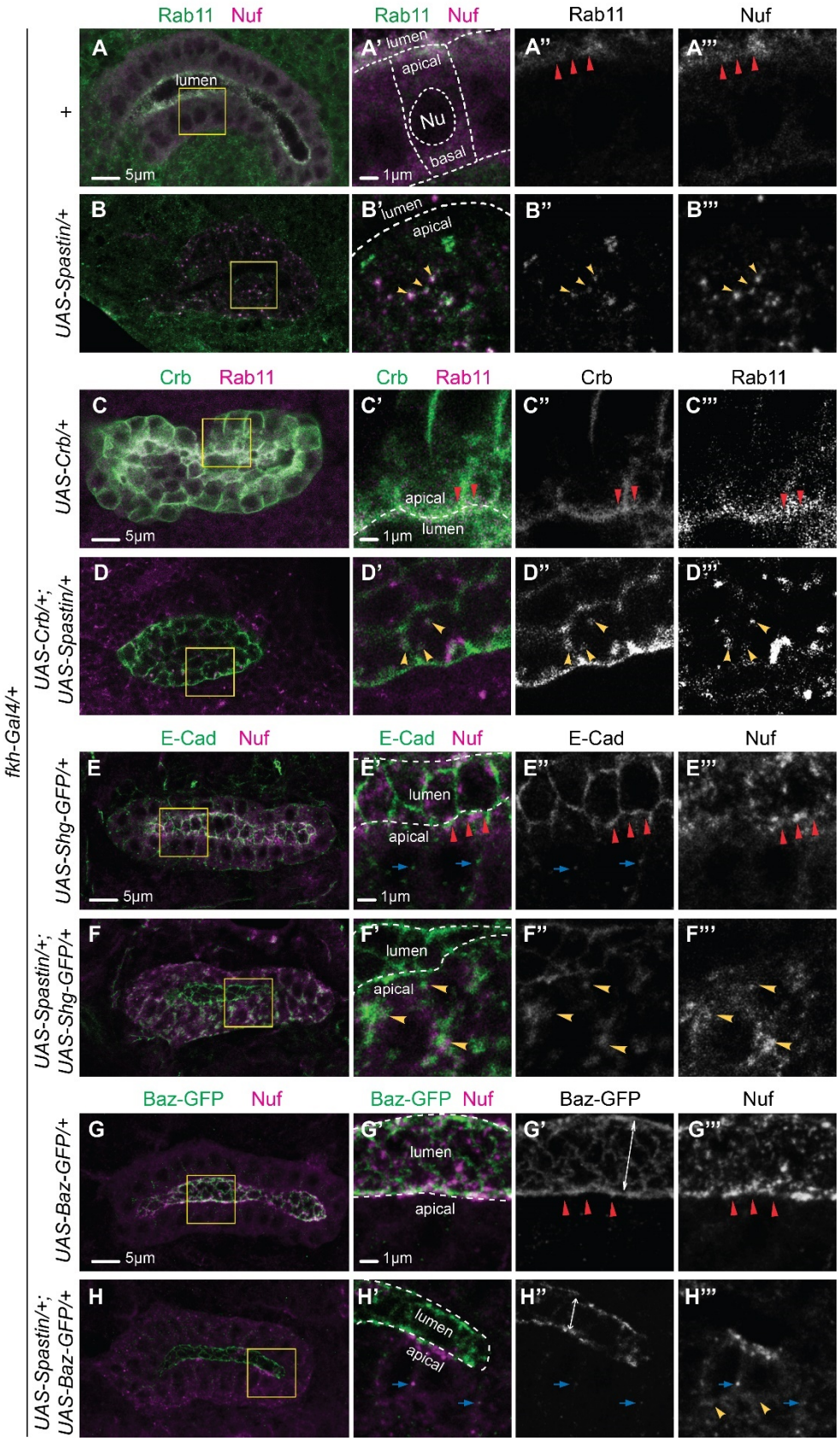

791

Supplemental Fig. 6: Fog does not colocalize with Nuf when MTs are disrupted. (A-A''') A stage 16 SG overexpressing Fog shows mislocalized Fog as cytoplasmic aggregates (yellow arrowheads). Nuf is still apically localized (red arrowheads). (B-B''') When Fog and spastin are co-overexpressed, mislocalized Fog is mainly observed in the basal region of cells. Nuf is mislocalized to the basolateral region of cells but does not overlap with Fog (yellow arrowheads). Nu: nucleus.

Supplemental Figure 6

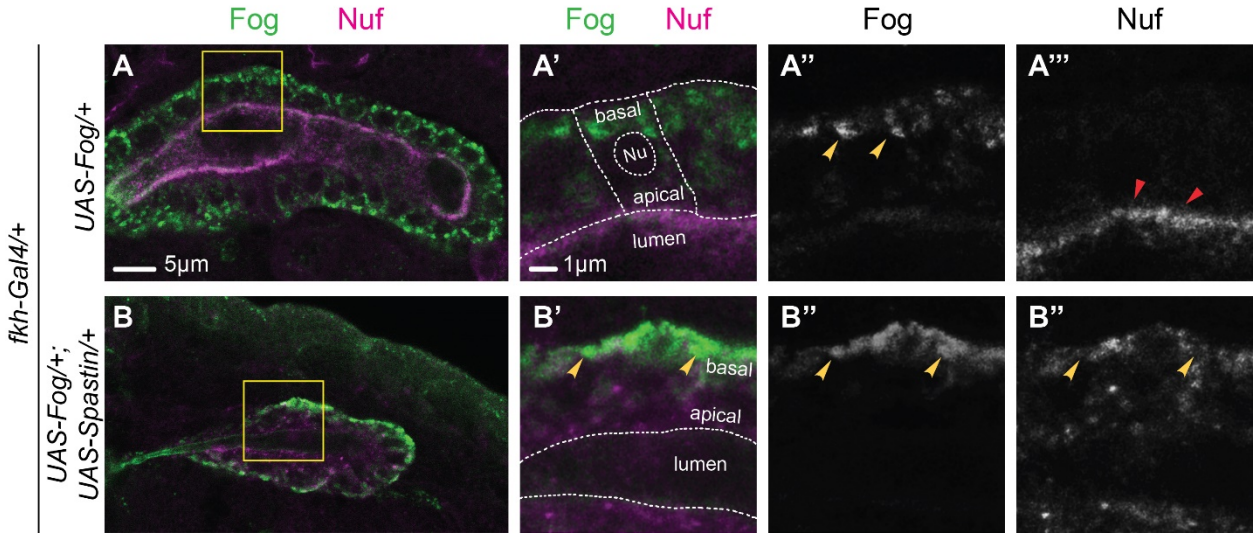

802 **Fly genotypes**

Figures	**Genotypes**
Figs. 1B-D', I-J'	Oregon R
Figs. 1F-H'	*Rab11-EYFP*
Figs. 1K-L'	*Rab7-EYFP*
Figs. 2A-B''	Oregon R
Figs. 2D-D'''	*fkh-Gal4/+*
Figs. 2E-E''', F-G''	*fkh-Gal4/UAS-Spastin-CFP*
Figs. 3A-A'	*fkh-Gal4/+*
Figs. 3B-B'	*fkh-Gal4/UAS-Rab11-S25N-YFP*
Figs. 3C-C'	*UAS-Dicer-2/+; fkh-Gal4/UAS-Dhc64C RNAi*
Figs. 3D-D'	Oregon R
Figs. 3E-E'	*klar*^{1}
Fig. 3G, first left panel (top and bottom)	*fkh-Gal4/+*
Fig. 3G, three right panels (top and bottom)	*matα-Gal4/+; fkh-Gal4/UAS-Dhc64C RNAi*
Figs. 4A-A''''	*sqh-GFP/+; fkh-Gal4/+*
Figs. 4B-B''''	*sqh-GFP/UAS-Dicer-2; fkh-Gal4/UAS-Dhc64C RNAi*
Figs. 4D-D''''	*sqh-GFP; sqh*^{AX3}
Figs. 4E-E''''	*sqh-GFP; klar*^{1}

Figs. 5A-A''	*fkh-Gal4 ubi-Rok-GFP/+*
Figs. 5B-B''	*UAS-Spastin; fkh-Gal4 ubi-Rok-GFP/+*
Figs. 5C-C''	*UAS-Dicer-2/+; fkh-Gal4 ubi-Rok-GFP/UAS-Dhc64C RNAi*
Figs. 5D-D''	*ubi-Rok-GFP*
Figs. 5E-E''	*klar^{mCD4} ubi-Rok-GFP*
Figs. 5F	*fkh-Gal4 ubi-Rok-GFP/+*
Figs. 6A-A'	*fkh-Gal4 ubi-Rok-GFP/+*
Figs. 6B-B'	*UAS-Fog/+; fkh-Gal4 ubi-Rok-GFP/+*
Figs. 6C-C'	*UAS-Fog/+; fkh-Gal4 ubi-Rok-GFP/UAS-Spastin*
Figs. 6D-D'	*UAS-Fog/+; fkh-Gal4 ubi-Rok-GFP/UAS-Dhc64C RNAi*
Figs. 6E-E'	*sqh-GFP/+; fkh-Gal4/+*
Figs. 6F-F'	*sqh-GFP/UAS-Fog; fkh-Gal4/+*
Figs. 6G-G'	*sqh-GFP/UAS-Fog; fkh-Gal4/UAS-Spastin*
Figs. 6H-H'	*sqh-GFP/UAS-Fog; fkh-Gal4/UAS-Dhc64C RNAi*
Figs. 6I-I'	*sqh-GFP/UAS-Fog; fkh-Gal4/+*
Figs. 7A-A'', C-C', E	*fkh-Gal4/+*
Figs. 7B-B'', D-D', F	*fkh-Gal4/UAS-Spastin*

Figs. 7L-L’	*fkh-Gal4/+*
Figs. 7M-M’	*fkh-Gal4/UAS-Crb RNAi*
Figs. 7N-N’	*fkh-Gal4/UAS-E-Cad RNAi*
Figs. 7O-O’	*fkh-Gal4/UAS-Baz RNAi*
Figs. 8A-A’’	*sqh-GFP/+; fkh-Gal4/+*
Figs. 8B-B’’	*sqh-GFP/+; fkh-Gal4/UAS-Crb RNAi*
Figs. 8C-C’’	*sqh-GFP/+; fkh-Gal4/UAS-E-Cad RNAi*
Figs. 8D-D’’	*sqh-GFP/+; fkh-Gal4/UAS-Baz RNAi*
Figs. 8F-F’’	*fkh-Gal4 ubi-Rok-GFP/+*
Figs. 8G-G’’	*fkh-Gal4 ubi-Rok-GFP/UAS-Crb RNAi*
Figs. 8H-H’’	*fkh-Gal4 ubi-Rok-GFP/UAS-E-Cad RNAi*
Figs. 8I-I’’	*fkh-Gal4 ubi-Rok-GFP/UAS-Baz RNAi*
Figs. S1A-B’	*Oregon R*
Figs. S1D-E’	*Rab5-EYFP*
Figs. S2A-A’’	*fkh-Gal4/+*
Figs. S2B-B’’	*fkh-Gal4/UAS-Spastin-CFP*
Figs. S3A,B,C	*fkh-Gal4/+*
Fig. S3A’	*fkh-Gal4/UAS-Crb* RNAi
Fig. S3B’	*fkh-Gal4/UAS-E-Cad* RNAi

Fig. S3C’	*fkh-Gal4/UAS-Baz* RNAi
Figs. S4A-A’	*fkh-Gal4/+*
Figs. S4B-B’	*UAS-Crb/+; fkh-Gal4/+*
Figs. S4C-C’	*UAS-Crb/+; fkh-Gal4/UAS-Spastin*
Figs. S5A-A’’’	*fkh-Gal4/+*
Figs. S5B-B’’’	*fkh-Gal4/UAS-Spastin*
Figs. S5C-C’’’	*UAS-Crb/+; fkh-Gal4/+*
Figs. S5D-D’’’	*UAS-Crb/+; fkh-Gal4/UAS-Spastin*
Figs. S5E-E’’’	*fkh-Gal4/UAS-Shg-GFP*
Figs. S5F-F’’’	*UAS-Spastin/+; fkh-Gal4/UAS-Shg-GFP*
Figs. S5G-G’’’	*fkh-Gal4/UAS-Baz-GFP*
Figs. S5H-H’’’	*UAS-Spastin/+; fkh-Gal4/UAS-Baz-GFP*
Figs. S6A-A’’’	*UAS-Fog/+; fkh-Gal4/+*
Figs. S6B-B’’’	*UAS-Fog/+; fkh-Gal4/UAS-Spastin*

803

804

805

806

807 **References**

808 Aguilar-Aragon, M., G. Fletcher and B. J. Thompson (2019). Apical transport of Crumbs
809 maintains epithelial cell polarity. Biorxiv.
810 Abreu-Blanco, M.T., Verboon, J.M., and Parkhurst, S.M. (2014). Coordination of Rho
811 family GTPase activities to orchestrate cytoskeleton responses during cell wound repair.
812 Curr Biol *24*, 144-155.
813 Anborgh, P.H., Seachrist, J.L., Dale, L.B., and Ferguson, S.S. (2000). Receptor/beta-
814 arrestin complex formation and the differential trafficking and resensitization of beta2-
815 adrenergic and angiotensin II type 1A receptors. Mol Endocrinol *14*, 2040-2053.
816 Andrew, D.J., and Ewald, A.J. (2010). Morphogenesis of epithelial tubes: Insights into
817 tube formation, elongation, and elaboration. Dev Biol *341*, 34-55.
818 Benton, M.A., Frey, N., Nunes da Fonseca, R., von Levetzow, C., Stappert, D.,
819 Hakeemi, M.S., Conrads, K.H., Pechmann, M., Panfilio, K.A., Lynch, J.A.*, et al.* (2019).
820 Fog signaling has diverse roles in epithelial morphogenesis in insects. Elife *8*.
821 Benton, R., and St Johnston, D. (2003). Drosophila PAR-1 and 14-3-3 inhibit
822 Bazooka/PAR-3 to establish complementary cortical domains in polarized cells. Cell
823 *115*, 691-704.
824 Booth, A.J.R., Blanchard, G.B., Adams, R.J., and Roper, K. (2014). A dynamic
825 microtubule cytoskeleton directs medial actomyosin function during tube formation. Dev
826 Cell *29*, 562-576.
827 Cerniello, F.M., Carretero, O.A., Longo Carbajosa, N.A., Cerrato, B.D., Santos, R.A.,
828 Grecco, H.E., and Gironacci, M.M. (2017). MAS1 Receptor Trafficking Involves ERK1/2
829 Activation Through a beta-Arrestin2-Dependent Pathway. Hypertension *70*, 982-989.
830 Chung, S., and Andrew, D.J. (2014). Cadherin 99C regulates apical expansion and cell
831 rearrangement during epithelial tube elongation. Development *141*, 1950-1960.
832 Chung, S., Hanlon, C.D., and Andrew, D.J. (2014). Building and specializing epithelial
833 tubular organs: the Drosophila salivary gland as a model system for revealing how
834 epithelial organs are specified, form and specialize. Wiley Interdiscip Rev Dev Biol *3*,
835 281-300.
836 Chung, S., Kim, S., and Andrew, D.J. (2017). Uncoupling apical constriction from tissue
837 invagination. Elife *6*.
838 Dale, L.B., Seachrist, J.L., Babwah, A.V., and Ferguson, S.S. (2004). Regulation of
839 angiotensin II type 1A receptor intracellular retention, degradation, and recycling by
840 Rab5, Rab7, and Rab11 GTPases. J Biol Chem *279*, 13110-13118.
841 David, D.J., Tishkina, A., and Harris, T.J. (2010). The PAR complex regulates pulsed
842 actomyosin contractions during amnioserosa apical constriction in Drosophila.
843 Development *137*, 1645-1655.
844 Dunst, S., Kazimiers, T., von Zadow, F., Jambor, H., Sagner, A., Brankatschk, B.,
845 Mahmoud, A., Spannl, S., Tomancak, P., Eaton, S.*, et al.* (2015). Endogenously tagged
846 rab proteins: a resource to study membrane trafficking in Drosophila. Dev Cell *33*, 351-
847 365.
848 Fan, G.H., Lapierre, L.A., Goldenring, J.R., and Richmond, A. (2003). Differential
849 regulation of CXCR2 trafficking by Rab GTPases. Blood *101*, 2115-2124.
850 Fuse, N., Yu, F., and Hirose, S. (2013). Gprk2 adjusts Fog signaling to organize cell
851 movements in Drosophila gastrulation. Development *140*, 4246-4255.

852 Gorvel, J.P., Chavrier, P., Zerial, M., and Gruenberg, J. (1991). rab5 controls early
853 endosome fusion in vitro. Cell *64*, 915-925.
854 Gross, S.P., Welte, M.A., Block, S.M., and Wieschaus, E.F. (2000). Dynein-mediated
855 cargo transport in vivo. A switch controls travel distance. J Cell Biol *148*, 945-956.
856 Guglielmi, G., Barry, J.D., Huber, W., and De Renzis, S. (2015). An Optogenetic Method
857 to Modulate Cell Contractility during Tissue Morphogenesis. Dev Cell *35*, 646-660.
858 Hamelin, E., Theriault, C., Laroche, G., and Parent, J.L. (2005). The intracellular
859 trafficking of the G protein-coupled receptor TPbeta depends on a direct interaction with
860 Rab11. J Biol Chem *280*, 36195-36205.
861 Hunyady, L., Baukal, A.J., Gaborik, Z., Olivares-Reyes, J.A., Bor, M., Szaszak, M.,
862 Lodge, R., Catt, K.J., and Balla, T. (2002). Differential PI 3-kinase dependence of early
863 and late phases of recycling of the internalized AT1 angiotensin receptor. J Cell Biol
864 *157*, 1211-1222.
865 Innamorati, G., Le Gouill, C., Balamotis, M., and Birnbaumer, M. (2001). The long and
866 the short cycle. Alternative intracellular routes for trafficking of G-protein-coupled
867 receptors. J Biol Chem *276*, 13096-13103.
868 Izquierdo, E., Quinkler, T., and De Renzis, S. (2018). Guided morphogenesis through
869 optogenetic activation of Rho signalling during early Drosophila embryogenesis. Nat
870 Commun *9*, 2366.
871 Jouette, J., Guichet, A., and Claret, S.B. (2019). Dynein-mediated transport and
872 membrane trafficking control PAR3 polarised distribution. Elife *8*.
873 Kerridge, S., Munjal, A., Philippe, J.M., Jha, A., de las Bayonas, A.G., Saurin, A.J., and
874 Lecuit, T. (2016). Modular activation of Rho1 by GPCR signalling imparts polarized
875 myosin II activation during morphogenesis. Nat Cell Biol *18*, 261-270.
876 Khanal, I., Elbediwy, A., Diaz de la Loza Mdel, C., Fletcher, G.C., and Thompson, B.J.
877 (2016). Shot and Patronin polarise microtubules to direct membrane traffic and
878 biogenesis of microvilli in epithelia. J Cell Sci *129*, 2651-2659.
879 Ko, C.S., Tserunyan, V., and Martin, A.C. (2019). Microtubules promote intercellular
880 contractile force transmission during tissue folding. J Cell Biol *218*, 2726-2742.
881 Laan, L., Pavin, N., Husson, J., Romet-Lemonne, G., van Duijn, M., Lopez, M.P., Vale,
882 R.D., Julicher, F., Reck-Peterson, S.L., and Dogterom, M. (2012). Cortical dynein
883 controls microtubule dynamics to generate pulling forces that position microtubule
884 asters. Cell *148*, 502-514.
885 Langevin, J., Morgan, M.J., Sibarita, J.B., Aresta, S., Murthy, M., Schwarz, T., Camonis,
886 J., and Bellaiche, Y. (2005). Drosophila exocyst components Sec5, Sec6, and Sec15
887 regulate DE-Cadherin trafficking from recycling endosomes to the plasma membrane.
888 Dev Cell *9*, 365-376.
889 Le Droguen, P.M., Claret, S., Guichet, A., and Brodu, V. (2015). Microtubule-dependent
890 apical restriction of recycling endosomes sustains adherens junctions during
891 morphogenesis of the Drosophila tracheal system. Development *142*, 363-374.
892 Lee, J.Y., and Harland, R.M. (2010). Endocytosis is required for efficient apical
893 constriction during Xenopus gastrulation. Curr Biol *20*, 253-258.
894 Letizia, A., Sotillos, S., Campuzano, S., and Llimargas, M. (2011). Regulated Crb
895 accumulation controls apical constriction and invagination in Drosophila tracheal cells. J
896 Cell Sci *124*, 240-251.

Li, M., McGrail, M., Serr, M., and Hays, T.S. (1994). Drosophila cytoplasmic dynein, a microtubule motor that is asymmetrically localized in the oocyte. J Cell Biol *126*, 1475-1494.
Manning, A.J., Peters, K.A., Peifer, M., and Rogers, S.L. (2013). Regulation of epithelial morphogenesis by the G protein-coupled receptor mist and its ligand fog. Sci Signal *6*, ra98.
Manning, A.J., and Rogers, S.L. (2014). The Fog signaling pathway: insights into signaling in morphogenesis. Dev Biol *394*, 6-14.
Martin, A.C., and Goldstein, B. (2014). Apical constriction: themes and variations on a cellular mechanism driving morphogenesis. Development *141*, 1987-1998.
Martin, A.C., Kaschube, M., and Wieschaus, E.F. (2009). Pulsed contractions of an actin-myosin network drive apical constriction. Nature *457*, 495-499.
Mason, F.M., Tworoger, M., and Martin, A.C. (2013). Apical domain polarization localizes actin-myosin activity to drive ratchet-like apical constriction. Nat Cell Biol *15*, 926-936.
Meresse, S., Gorvel, J.P., and Chavrier, P. (1995). The rab7 GTPase resides on a vesicular compartment connected to lysosomes. J Cell Sci *108 (Pt 11)*, 3349-3358.
Miao, H., Vanderleest, T.E., Jewett, C.E., Loerke, D., and Blankenship, J.T. (2019). Cell ratcheting through the Sbf RabGEF directs force balancing and stepped apical constriction. J Cell Biol.
Myat, M.M., and Andrew, D.J. (2000). Organ shape in the Drosophila salivary gland is controlled by regulated, sequential internalization of the primordia. Development *127*, 679-691.
Myat, M.M., and Andrew, D.J. (2002). Epithelial tube morphology is determined by the polarized growth and delivery of apical membrane. Cell *111*, 879-891.
Ossipova, O., Kim, K., Lake, B.B., Itoh, K., Ioannou, A., and Sokol, S.Y. (2014). Role of Rab11 in planar cell polarity and apical constriction during vertebrate neural tube closure. Nat Commun *5*, 3734.
Rauzi, M., Lenne, P.F., and Lecuit, T. (2010). Planar polarized actomyosin contractile flows control epithelial junction remodelling. Nature *468*, 1110-1114.
Riggs, B., Rothwell, W., Mische, S., Hickson, G.R., Matheson, J., Hays, T.S., Gould, G.W., and Sullivan, W. (2003). Actin cytoskeleton remodeling during early Drosophila furrow formation requires recycling endosomal components Nuclear-fallout and Rab11. J Cell Biol *163*, 143-154.
Roeth, J.F., Sawyer, J.K., Wilner, D.A., and Peifer, M. (2009). Rab11 helps maintain apical crumbs and adherens junctions in the Drosophila embryonic ectoderm. PLoS One *4*, e7634.
Roper, K. (2012). Anisotropy of Crumbs and aPKC drives myosin cable assembly during tube formation. Dev Cell *23*, 939-953.
Royou, A., Field, C., Sisson, J.C., Sullivan, W., and Karess, R. (2004). Reassessing the role and dynamics of nonmuscle myosin II during furrow formation in early Drosophila embryos. Mol Biol Cell *15*, 838-850.
Sanchez-Corrales, Y.E., Blanchard, G.B., and Roper, K. (2018). Radially patterned cell behaviours during tube budding from an epithelium. Elife *7*.

941 Sawyer, J.M., Harrell, J.R., Shemer, G., Sullivan-Brown, J., Roh-Johnson, M., and
942 Goldstein, B. (2010). Apical constriction: a cell shape change that can drive
943 morphogenesis. Dev Biol *341*, 5-19.
944 Sherwood, N.T., Sun, Q., Xue, M., Zhang, B., and Zinn, K. (2004). Drosophila spastin
945 regulates synaptic microtubule networks and is required for normal motor function.
946 PLoS Biol *2*, e429.
947 Sidor, C., Stevens, T.J., Jin, L., Boulanger, J., and Roper, K. (2020). Rho-Kinase Planar
948 Polarization at Tissue Boundaries Depends on Phospho-regulation of Membrane
949 Residence Time. Dev Cell *52*, 364-378 e367.
950 Ullrich, O., Reinsch, S., Urbe, S., Zerial, M., and Parton, R.G. (1996). Rab11 regulates
951 recycling through the pericentriolar recycling endosome. J Cell Biol *135*, 913-924.
952 Urbansky, S., Gonzalez Avalos, P., Wosch, M., and Lemke, S. (2016). Folded
953 gastrulation and T48 drive the evolution of coordinated mesoderm internalization in flies.
954 Elife *5*.
955 Volpicelli, L.A., Lah, J.J., Fang, G., Goldenring, J.R., and Levey, A.I. (2002). Rab11a
956 and myosin Vb regulate recycling of the M4 muscarinic acetylcholine receptor. J
957 Neurosci *22*, 9776-9784.
958 Westermann, S., and Weber, K. (2003). Post-translational modifications regulate
959 microtubule function. Nat Rev Mol Cell Biol *4*, 938-947.
960 Wichmann, H., Hengst, L., and Gallwitz, D. (1992). Endocytosis in yeast: evidence for
961 the involvement of a small GTP-binding protein (Ypt7p). Cell *71*, 1131-1142.
962 Wodarz, A., Grawe, F., and Knust, E. (1993). CRUMBS is involved in the control of
963 apical protein targeting during Drosophila epithelial development. Mech Dev *44*, 175-
964 187.
965 Yvon, A.M., Gross, D.J., and Wadsworth, P. (2001). Antagonistic forces generated by
966 myosin II and cytoplasmic dynein regulate microtubule turnover, movement, and
967 organization in interphase cells. Proc Natl Acad Sci U S A *98*, 8656-8661.
968 Zhang, X.M., Ellis, S., Sriratana, A., Mitchell, C.A., and Rowe, T. (2004). Sec15 is an
969 effector for the Rab11 GTPase in mammalian cells. J Biol Chem *279*, 43027-43034.

970